

1 **Expanding seawater carbon dioxide and methane measuring capabilities with a Seaglider**

2

3 Claudine Hauri^{1*}, Brita Irving¹, Dan Hayes², Ehsan Abdi^{3,4}, Jöran Kemme⁵, Nadja Kinski⁵, and

4 Andrew M. P. McDonnell^{6,7}

Deleted: 1

5

6 ¹International Arctic Research Center, University of Alaska Fairbanks, Fairbanks, AK 99775,

7 USA

8 ²Advanced Offshore Operations, Inc., Houston, TX 77004, USA

9 ³Cyprus Subsea Consulting and Services, Lakatamia 2326, Cyprus

10 ⁴now at Akvaplan-Niva, 9296 Tromsø, Norway

11 ⁵-4H-JENA engineering GmbH, 07745 Jena, Germany

12 ⁶ College of Fisheries and Ocean Science, University of Alaska Fairbanks, Fairbanks, AK 99775,

13 USA

14 ⁷now at Alaska Renewables, Fairbanks, AK 99709, USA

15

16 Corresponding author: Claudine Hauri (chauri@alaska.edu)

18 **Abstract**

19 Warming, ocean acidification, and deoxygenation are increasingly putting pressure on
20 marine ecosystems. At the same time, thawing permafrost and decomposing hydrates in Arctic
21 shelf seas may release large amounts of methane (CH₄) into the water column, which could
22 accelerate local ocean acidification and contribute to climate change. The key parameters to
23 observing and understanding these complex processes and feedback mechanisms are vastly
24 undersampled throughout the oceans. We developed carbon dioxide (CO₂) and CH₄ gliders,
25 including standard operational procedures with the goal that CO₂ and CH₄ measurements become
26 more common for glider operations. The Seagliders with integrated Contros HydroC CO₂ or CH₄
27 sensors also include conductivity, temperature, depth, oxygen, chlorophyll-a, backscatter, and
28 fluorescent dissolved organic matter sensors. Communication via satellite allows for near-real
29 time data transmission, sensor adjustments, and adaptive sampling. Several sea trials with the
30 CO₂ Seaglider in the Gulf of Alaska and data evaluation with discrete water and underway
31 samples suggest near 'weather quality' CO₂ data as defined by the Global Ocean Acidification
32 Network. A winter mission in Resurrection Bay, Alaska ~~provided~~ first insights into the water
33 column inorganic carbon dynamics during this otherwise undersampled season. The CH₄
34 Seaglider passed its flight trials in Resurrection Bay. ~~yet needs to be tested during a field mission~~
35 ~~in an area with CH₄ concentrations beyond background noise~~. Both sensing systems are available
36 to the science community through the industry partners (Advanced Offshore Operations and -4H-
37 ~~JENA,engineering GmbH~~) of this project.

Deleted: provides

Deleted: but yet

Deleted: and is ready to be deployed in an area with greater CH₄ activity

Deleted: JENA

38
39 **1. Introduction**

45 Understanding the distribution and dynamics of carbon dioxide (CO₂) and methane (CH₄)
46 in the ocean is crucial for predicting and mitigating climate change and ocean acidification
47 impacts. Within the ocean, CO₂ levels (measured as the partial pressure of CO₂, pCO₂ and/or
48 fugacity of CO₂) are spatially and temporally variable as they are influenced by a myriad of
49 highly dynamic physical, chemical, and biological processes. On top of this natural variability,
50 the ocean has absorbed about one third of the CO₂ emitted by humans since the industrial
51 revolution (Sabine et al., 2004; Gruber et al., 2019). In doing so, it has played an important role
52 in mitigating climate change (Sabine and Tanhua, 2010). However, both the oceanic uptake of
53 anthropogenic CO₂ and climate change are altering the distribution of oceanic CO₂ and are
54 causing ocean acidification (Doney et al., 2009; Qi et al., 2022; Woosley and Millero, 2020). At
55 the same time, the oceans are warming and losing oxygen (Johnson and Lyman, 2020; Breitburg
56 et al., 2018), increasing the stress on marine ecosystems. As these long-term changes unfold,
57 marine heat waves, and high acidity or low oxygen extreme events will last longer, become more
58 intense, and happen more often and at the same time (Laufkötter et al., 2020; Gruber et al., 2021;
59 Hauri et al., 2024). Negative effects on certain organisms are even stronger if exposed to a
60 combination of different stressors (Breitberg et al., 2015; Kroeker et al., 2017).

61 Over 100 years, CH₄ possesses a global warming potential approximately 28 times
62 greater than that of CO₂ (IPCC AR5; Myhre et al., 2013). Sediments along the seafloor at
63 continental margins contain large amounts of CH₄, with about ten times as much carbon as the
64 atmosphere (Kessler, 2014). CH₄ is biologically produced in anoxic sediments and the surface
65 mixed layer or released from geological sources like hydrocarbon seeps and degrading methane
66 hydrate deposits (Barnes and Goldberg; Du et al, Skarke 2014). This powerful greenhouse gas is
67 emitted to the atmosphere through bubbling (ebullition) or diffusive gas transfer (Reeburgh,

Formatted: Subscript

Formatted: Subscript

Deleted: The oceanic reservoir of carbon dioxide (CO₂) is large, dynamic, spatially variable, and of critical importance to Earth's climate, biogeochemical cycles, and the health of marine ecosystems.

Formatted: Subscript

Deleted: over a 100-year period that is

Formatted: Font: Not Bold

Deleted: than

Formatted: Font: Not Bold

74 2007; McGinnis et al., 2006), which is limited by rapid oxidation to CO₂ during transport
75 through the water column (Leonte et al., 2017). CH₄ occurs generally at low levels (background
76 concentrations) throughout oceans, unless close to a source. Positive feedback mechanisms, like
77 warming induced CH₄ seepage from destabilizing hydrates and thawing subsea permafrost, may
78 further accelerate ocean acidification and climate change (Garcia-Tigreros et al., 2021; Sparrow
79 et al., 2018; Shakhova et al., 2010; Rees et al., 2022).

80 To effectively observe and understand the complex processes and feedback mechanisms
81 regulating Earth's systems, certain key parameters, defined by the Global Ocean Observing
82 System as essential ocean variables, must be measured accurately. However, these variables are
83 often vastly undersampled across time and space due to traditional sampling methods, which rely
84 mainly on discrete water sample collections from dedicated research cruises, underway
85 measurements from transiting vessels, or time series measurements from in situ sensors on fixed
86 moorings. Although biogeochemical sensors deployed on autonomous platforms like moorings
87 and Argo floats have become more prevalent, challenges such as high power requirements,
88 sensor size, and data quality hinder their widespread use on underwater gliders. Autonomous,
89 spatially resolved surface measurements of pCO₂ and pH are collected using wave gliders and
90 sail drones (Chavez et al., 2018; Nickford et al., 2022; Manley and Willcox, 2010). The state-of-
91 the-art biogeochemical (BGC) Argo floats measure variables like pH, O₂, NO₃, chlorophyll-a,
92 suspended particles, and downwelling irradiance in subsurface waters (Claustre et al., 2020).
93 These floats can last several years at low sampling resolutions, such as a 2000-meter depth
94 profile every ten days, or they can be programmed for high-resolution and shallow sampling.
95 They can even sample beneath seasonal sea ice (Briggs et al., 2018). Despite their capabilities,

Formatted: Font: Not Bold

Field Code Changed

Deleted: Positive feedback mechanisms, like warming induced CH₄ seepage from destabilizing hydrates and thawing subsea permafrost, may further accelerate ocean acidification and climate change (Garcia-Tigreros et al., 2021; Sparrow et al., 2018; Shakhova et al., 2010; Rees et al., 2022). ¶

Formatted: Font: Not Bold

Formatted: Font: Not Bold

Formatted: Font: Not Bold

Formatted: Indent: First line: 0.5", Line spacing: Double

Deleted: (EOVs,)

Formatted: Font: Not Bold

Formatted: Font: Not Bold

Deleted: in recent years

Formatted: Font: Italic

Formatted: Subscript

Formatted: Subscript

Formatted: Subscript

Deleted: for

105 their trajectory is hard to control, and they are usually not recovered after their mission, which
106 prevents sensor calibration and post-mission corrections.
107 Ocean gliders autonomously collect water column data along planned waypoints, which
108 allows for controlled exploration and adaptive sampling. To date, pH is the only carbon system
109 parameter that has been successfully integrated into ocean gliders (Hemming et al., 2017; Saba et
110 al., 2019; Possenti et al., 2021; Takeshita et al., 2021). The most promising results came from
111 ISFET based pH sensors (Saba et al., 2019; Wright-Fairbanks et al., 2020; Takeshita et al.,
112 2021). However, ISFET-based pH sensors require significant conditioning periods before
113 deployment, suffer from biofouling, require annual cleaning and calibration at the manufacturer,
114 and careful discrete sample collection at deployment and recovery to characterize and correct for
115 sensor drift (Thompson et al., 2021). There have been few attempts to integrate $p\text{CO}_2$ sensors
116 into gliders (Hemming et al., 2017; Hauri et al., 2018; von Oppeln-Bronikowski et al., 2021).
117 Hemming et al. (2017) did not publish the data because of low quality. Von Oppeln-Bronikowski
118 et al. (2021) integrated an Aanderaa CO_2 optode that measures $p\text{CO}_2$ by detecting the
119 luminescent quenching response from a CO_2 -sensitive membrane with a Slocum G2 glider but
120 suffered from instability, thermal-lag issues, variable conditioning periods (4 days to 1 month),
121 large offsets (> 1000 uatm), nonlinear temperature-dependent response time, and a high
122 dependence on prior foil calibration. Hauri et al. (2018) integrated the Pro Oceanus Mini Pro
123 CO_2 sensor with a Slocum G2. However, the Pro Oceanus Mini Pro CO_2 sensor used at the time
124 did not withstand the pressure changes imposed by glider missions. The Franatech METS CH_4
125 sensor has been integrated into Alseamar SeaExplorer and Teledyne Slocum gliders and
126 successfully used to generate concentration maps of a methane seep in a semi-quantitative way
127 (Meurer et al., 2021).

Deleted: The key parameters to observing and understanding these complex processes and feedback mechanisms are vastly undersampled throughout the oceans owing to conventional sampling approaches that rely primarily on discrete water sample collections from dedicated research cruises, underway measurements of surface ocean properties from transiting vessels, or time series measurements from in situ sensors on fixed moorings. Biogeochemical sensors deployed on autonomous platforms have become more commonly used but power requirements, long conditioning periods, sensor stability, drift, size, data quality, biofouling, and the need for discrete sample validation and calibration in the field continue to present significant obstacles to widespread adoption and utilization. Autonomous and spatially highly resolved surface measurements of $p\text{CO}_2$ and pH are collected with wave gliders and sail drones (Chavez et al., 2018; Nickford et al., 2022; Manley and Willcox, 2010). Biogeochemical Argo floats are the state of the art autonomous platform to measure a subset of these variables, including pH, O_2 , NO_3 , chlorophyll- a , suspended particles, and downwelling irradiance in subsurface waters (Claustre et al., 2020). BGC Argo floats can last for several years at low sampling resolution, e.g. a 2000 m depth profile every ten days, or they can be programmed for high resolution and shallow sampling as well. The floats can also sample underneath seasonal sea ice (Briggs et al., 2018). However, their trajectory cannot be easily manipulated, and they are not typically recovered at the end of their mission, which prevents sensor calibration and post-mission corrections.

Deleted: Ocean gliders autonomously collect water column data along planned waypoints, which allows for controlled exploration and adaptive sampling. A variety of pH sensors have been integrated into ocean gliders

Deleted: ,

Deleted: with the most promising results from ISFET based pH sensors...

Deleted: ISFET

Deleted: prior to

Deleted: as well as

Deleted: was so low

Deleted: through

Deleted: The highest quality CO_2 sensors rely on membrane equilibration and NDIR spectrometry.

Formatted: Font color: Black

171 Here we integrated modified versions of the Contros HydroC CO₂ and CH₄ sensors with
172 a Seagliders® (registered trademark of the University of Washington). We discuss details of the
173 physical and software integration, present CO₂ and CH₄ data from tank experiments, evaluate the
174 quality of pCO₂ data collected during CO₂ Seagliders missions, and discuss highlights from
175 missions in Resurrection Bay, Alaska.

176

177 2. Methods

178 2.1 CO₂ Seagliders

179 We integrated a modified version (Seagliders (SG) HydroC CO₂) of the CONTROS
180 HydroC™ CO₂ sensor (-4H-JENA engineering GmbH, Kiel, Germany) with a Seagliders M1
181 (Figure 1 a and b). The Seagliders M1 ~~was~~ specifically designed for long endurance missions in
182 deep waters to 1000 m depth. The HydroC CO₂ sensor ~~was outfitted with~~ a semi-permeable
183 TOUGH membrane (Pinnau and Toy, 1996) that ~~equilibrated~~ dissolved CO₂ between the ambient
184 seawater and the headspace of the sensor, where the gas concentration ~~was~~ determined by
185 nondispersive infrared (NDIR) spectrometry.

186 ~~Since the equilibration time (response time) of membrane-based sensors is affected by the~~
187 exchange of the water mass in front of the sensor head, we installed a Seabird Electronics (SBE)
188 5M pump next to the SG HydroC CO₂ sensor using tubing to transfer seawater from outside the
189 gliders fairing to the membrane surface (Figure 1a). The response time was determined at the
190 manufacturer, verified in the field, and then used to correct for hysteresis during the post-
191 processing phase (see [Section 2.7.2](#)).

192 The form factor of the HydroC CO₂™ sensor and Seagliders were changed to achieve an
193 internal integration of the sensor with the Seagliders. The standard ~~high~~-performance HydroC

Deleted:

Formatted: Indent: First line: 0.5", Line spacing: Double

Deleted: E

Deleted: is

Deleted: has

Deleted: equilibrates

Deleted: is

Deleted: The sensor has a zero-signal function (Fietzek et al., 2014),

Formatted: Font color: Black

Deleted: which allows for post mission correction of potential instrument drift and determination of in situ sensor response time. More technical details about the sensor and its performance are described in Fietzek et al., (2014).

Deleted: section

Deleted: high

208 CO₂TM sensor was changed from ø 89 x 380 mm to ø 136 x 294 mm by rearranging the gas-cycle
209 components and the control unit (Figure 1c). This new SG HydroC CO₂ sensor is available in
210 polyoxymethylene (POM) cladding rated to 300 m or a titanium housing rated to 1000 m to
211 provide a choice between a coastal mission and an offshore deeper mission. Use of the titanium
212 housing required a syntactic foam housing to compensate for the weight, whereas the POM
213 housing was integrated into the glider with simple brackets (Figure 2). Despite these adjustments
214 to the size of the sensor, to our knowledge, it is still the largest and heaviest sensor that has been
215 integrated with a Seaglider to date. The forward fairing of the Seaglider was extended by 40 cm
216 with a fiberglass cylindrical extension to create internal wet payload space for the sensor, pump,
217 and cables (Figure 1 a and b). The sensor was mounted with the membrane facing aft to ensure
218 that potential bubbles within the internal tubing of the sensor could escape the system during the
219 downcast of the first dive. In situ comparison of the orientation of the sensor and close
220 examination of pCO₂ and internal pressure data suggested the highest data quality was achieved
221 with this mounting design.
222 One of the advantages of using ocean gliders for ocean observing is the ability for real-
223 time communication of data and commands between the pilot and the glider. To take advantage
224 of this, modifications were needed to allow two-way communication between the Seaglider
225 firmware and the HydroC firmware. The Seaglider firmware has a feature to allow easy
226 integration of “logging devices,” which provides a way to build commands for the pilot on land
227 to switch the sensor on and off and change sampling strategy during the mission (on/off below or
228 above certain depth) when it comes to the surface for a communication session. The Seaglider
229 firmware can also automatically set the clock of the sensor on request at every surfacing and
230 send small samples of the data stream via Iridium along with the standard sensor data. This

Deleted: requires

Deleted: can be

Formatted: Font: 12 pt, Not Bold, Not Italic

Deleted: is

Formatted: Font: 12 pt, Not Bold, Not Italic

Formatted: Font: 12 pt

Formatted: Font: 12 pt, Not Bold, Not Italic

Deleted: from the HydroC oriented with the membrane facing forward...

Deleted: In situ comparison of the orientation of the sensor suggested the highest data quality is achieved with this mounting design.

Formatted: Font: 11 pt, Bold, Font color: Black

Formatted: Line spacing: Double

239 required the writing and testing of a driver file (CNF file). However, to take full advantage of the
240 ability of the HydroC, a more-advanced electronic integration was carried out using Smart
241 Interoperable Real-time Maritime Assembly (SIRMA™, registered trademark of Cyprus Subsea
242 Consulting and Services, C.S.C.S., Ltd.). This small programmable electronic circuit ~~contained~~
243 hardware elements to adapt the sensor power and communication requirements to those available
244 on the host platform. It also ~~allowed~~ for separate storage and processing capabilities to
245 supplement the main host processor that controls the flight, sampling, and telecommunications of
246 the host. Most importantly here, it was programmed to relay pilot commands to the SG HydroC
247 CO₂ for the built-in “zero” function, which ~~isolated~~ the internal gas circuit until there ~~was~~ no
248 CO₂ present, ~~measured~~ the concentration signal, and ~~assigned~~ a zero value. Then the gas circuit
249 ~~was~~ exposed to the headspace behind the diffusion membrane for in situ sampling. SIRMA was
250 also programmed to extract raw data from the HydroC and calculate ~~the~~ bin average of some of
251 the output fields, which ~~were~~ useful for real-time mission adaptation and confirmation of sensor
252 operation. Three levels of output were allowed, depending on how much surfacing time could be
253 tolerated before continuing the mission (Baud rate for Iridium is very low, on the order of 4800
254 bps). ~~More detailed information can be found in the CO₂ Seaglider SOP (Irving et al., 2024).~~

255 In addition to the HydroC CO₂ sensor, the CO₂ Seaglider carried an Aanderaa 4831F
256 optode, a compact optical oxygen sensor, which ~~works~~ on the principle of luminescence
257 quenching by oxygen. The 4831F ~~was~~ equipped with a fast response sensing foil with a ~~well-~~
258 characterized response time of 8 seconds. ~~The~~ Aanderaa optode ~~measured~~ absolute oxygen
259 concentration and ~~percentage~~ saturation. ~~It is~~ the most widely used on ocean gliders, and ~~has~~ been
260 integrated into both Slocum and Seagliders (OceanGliders Oxygen SOP, 2024; Bittig et al.,
261 2018). The OceanGliders community has developed a Standard Operating Procedure (SOP) that

Deleted: contains

Deleted: allows

Deleted: isolates

Deleted: i

Deleted: measures

Deleted: assigns

Deleted: is

Deleted:

Deleted: are

Commented [B11]: It's not actually part of OceanGliders, so we can't claim that 😊 hopefully in the future they'll take it over.

Deleted: OceanGlider

Deleted: our

Deleted: [https://github.com/britairving/Carbon_Dioxide_SO P...](https://github.com/britairving/Carbon_Dioxide_SO_P...)

Formatted: Highlight

Deleted: CITE

Formatted: Highlight

Formatted: Indent: First line: 0.5", Line spacing: Double

Deleted: works

Deleted: ed

Deleted: is

Deleted: well

Deleted: s

Deleted: %

Deleted: ,

Deleted: are

Deleted: ,

Deleted: have

286 details everything from mounting, calibration, available sensors, piloting tips, [and](#) response time
287 correction, to post-processing (OceanGliders Oxygen SOP, 2024). The CO₂ Seaglider was also
288 outfitted with an SBE CT sail and Wetlabs Ecopuck [measuring chlorophyll fluorescence at 695](#)
289 [nm](#).

Formatted: Font: 12 pt, Not Bold

Deleted: .

Deleted: ¶

291 2.2 CH₄ Seaglider

292 We also integrated a modified version of the CONTROS HydroC CH₄ sensor (-4H-JENA
293 [engineering](#) GmbH, Kiel, Germany) with the Seaglider. [The manufacturer's published](#)
294 [uncertainty of the HydroC CH₄ sensor is 2 µatm or ± 3 %, whichever is greater](#). The SG HydroC
295 CH₄ sensor [had](#) the same form factor as the SG HydroC CO₂ sensor. [However, it was 0.5 kg](#)
296 heavier [due to its](#) Tunable Diode Laser Absorption Spectroscopy (TDLAS) component, so the
297 SG HydroC CH₄ [had to](#) be integrated with changes to the glider's ballast.

Deleted: engineering

Deleted: (Figure 4c, shaded gray).

Deleted:

Deleted: has

Deleted: ,

Deleted: h

Deleted: is

Deleted: was

Deleted: with its

Deleted: must

299 2.3 Spring and winter CO₂ Seaglider missions

300 Both versions of the CO₂ Seaglider (rated to 300 m versus 1000 m) were tested in
301 separate missions ([Figure 3, Table S1](#)) in spring ([53 dives, May 4 – 7, 2022, Figure 5](#)) and winter
302 ([310 dives, February 8 – 21, 2023, Figure 6](#)). The 300 m version with integrated POM housing
303 was tested during a five-[day](#)-long mission in May 2022. The glider followed along a transect
304 within Resurrection Bay. CTD casts near the glider path allowed for [in](#)-depth evaluation of the
305 data quality. The 1000 m [depth](#)-rated CO₂ Seaglider with integrated titanium housing was tested
306 in February 2023. [Estimated energy consumption during the CO₂ Seaglider missions was 19 out](#)
307 [of 135 Ah and 75 out of 120 Ah for the 24 V which powered the SG HydroC CO₂ sensor battery](#)
308 [for the spring and winter missions, respectively. Before the February mission, the on board](#)

Formatted: Line spacing: Double

Deleted: (Figure 3).

Deleted: day

Deleted: in

Deleted: (Table 2 and Figure 2)

Deleted: depth

Formatted: Font: 12 pt

Formatted: Font: 12 pt

Formatted: Font: 12 pt, Font color: Auto

326 ~~modem was replaced with a newer model, with different input voltage requirements, which were~~
327 ~~probably not met as the mission evolved. As a result, the glider could not communicate and was~~
328 ~~lost. While this was an unfortunate mistake, the loss of the glider had nothing to do with the~~
329 ~~HydroC CO₂ integration.~~

Deleted: different

Deleted: anymore

Formatted: Font: 12 pt

Formatted: Font: 12 pt, Subscript

Formatted: Font: 12 pt

331 2.4 Tank experiments

332 ~~Shortly before the May 2022 glider mission, the glider was kept in a flow-through tank at~~
333 ~~the Alutiiq Pride Marine Institute for roughly 12 h for cross-calibration purposes.~~ The flow-
334 ~~through tank was fed with water from about 75 m depth and 91 m from the laboratory into~~
335 ~~Resurrection Bay, near a freshwater source. During the tank experiment, SG HydroC CO₂T-~~
336 ~~0718-001 (Figure 4b, blue line) was integrated into the Seaglider, and SG HydroC CO₂T-0422-~~
337 ~~001 (Figure 4b, black line) and the SG HydroC CH₄ (Figure 4c) sensors were secured next to the~~
338 ~~Seaglider. The water was kept in motion with a circulation pump. Triplicate discrete water~~
339 ~~samples for dissolved inorganic carbon, pH, and CH₄ analysis were taken every four hours~~
340 ~~(Table 1).~~

Deleted: T

Deleted: 4a

Deleted: .

Deleted: installed on rocks

342 2.5 Rosette package

343 ~~One of the SG HydroC CO₂ sensors (CO₂T-0422-001) was installed on an SBE-55 frame~~
344 ~~ECO water sampler with six 4-liter sample bottles (Seabird Scientific) during the May 2022 trials~~
345 ~~(Tables 2 and 3, Figure 7 and S1). The SBE-55 and SG HydroC CO₂ were powered by an SBE-~~
346 ~~33 carousel deck unit. The SG HydroC CO₂ interfered with the communication stream and~~
347 ~~thereby prevented real-time data acquisition and control of the SBE-55, however data were~~
348 ~~internally logged. The depth of the rosette package was monitored directly on the winch and the~~

Deleted: The spare

Deleted: controlled and

Deleted: a

Formatted: Font: 12 pt, Not Bold, Not Italic

Formatted: Font: 12 pt, Not Bold, Not Italic, Subscript

Formatted: Font: 12 pt, Not Bold, Not Italic

Deleted: The SG HydroC CO₂ interfered with the communication stream and thereby prevented real-time data acquisition and control of the SBE-55, however data were internally logged as required. D

362 timing of firing of the sample bottles, after an approximate 15-minute hovering period (to allow
363 for equilibration), was programmed in advance based on time intervals. On May 3 (Table 2,
364 Figure 7) only samples from the upper 20 m of the water column were usable due to issues with
365 manually measuring the depths and the sample collection. On May 7 (Table 3, Figure S1) two
366 bottles that were intended to be fired while the rosette was stationary at depth, were instead fired
367 while the rosette was in motion.

Deleted: min

Deleted: during the upcast

Deleted: Target depths for discrete water sample collection were 5 m, 20 m, 40 m, 60 m, and 80 m. However,

Commented [B12]: Does this sound okay? I removed the specific depths you listed because we now show both casts.

Deleted: ¶

369 2.6 Discrete water samples

370 2.6.1 Inorganic carbon chemistry

371 Discrete seawater samples were collected for sensor validation in two different cases in
372 May of 2022. Firstly, samples were taken alongside two SG HydroC CO₂ sensors during a tank
373 experiment at the Alutiiq Pride Marine Institute (Figure 4b, Table 1), from adjacent sample
374 bottles (Figure 1d). Secondly, samples were taken from bottles during a CTD cast within 1 km
375 and 4 hours of the HydroC measuring pCO₂ on the glider while conducting dives (Section 3.2).

376 Inorganic carbon sampling in the Gulf of Alaska's glaciated coastal regions required
377 methodological variations from open-ocean best practices to ensure that suspended mineral
378 particles do not compromise the instrumentation and/or bias measurements between sample
379 collection and analysis (Sejr et al., 2011). Given this, the discrete seawater samples were filtered
380 (replaceable 0.45 µm filter in a 47 mm polycarbonate in-line filter) with a peristaltic pump
381 straight from the Niskin bottles (see Bockmon and Dickson, (2014) for detailed method), or tank,
382 into pre-cleaned 500 mL borosilicate bottles, and poisoned with 200 µL mercuric chloride
383 (HgCl₂) (Dickson et al., 2007). Samples were transported and stored at room temperature before
384 analysis. Samples were opened immediately (<10 minutes) before concurrent analyses of pH

Deleted: Discrete seawater samples were collected for sensor validation alongside two SG HydroC CO₂ sensors during a tank experiment at the Alutiiq Pride Marine Institute (Figure 4ba, Table 1), from sample bottles mounted next to the SG HydroC CO₂ (Figure 1d), and from sample bottles during a CTD cast within 500 1 km and 30-60 minutes4 hours of the HydroC measuring pCO₂ on the glider while conducting dives (Section 3.2).¶

Deleted:

Deleted: requires

Deleted: ,

Deleted: 5

402 and DIC to limit gas exchange with ambient lab conditions. Samples were analyzed for DIC
403 using an Apollo SciTech, LLC Dissolved Inorganic Carbon Analyzer model AS-C6. All species
404 of dissolved inorganic carbon in a sample were converted to CO₂ by the addition of a strong acid.
405 The CO₂ gas was then purged from the sample through a drying system. The concentration of
406 CO₂ gas was measured using a non-dispersive infrared gas analyzer, the LI-7000 CO₂/H₂O
407 Analyzer. This method required Certified Reference Material (CRM, Batch #198 from A.
408 Dickson's Certified Reference Materials Laboratory) to create a three-point calibration line. The
409 calibration line was used to quantify the total amount of CO₂ in the sample as the integrated area
410 under the concentration-time curve. Apollo SciTech recommendations to improve analytical
411 accuracy were followed and included bubbling of CO₂ off the acid daily, allowing the analyzer to
412 warm up for at least 2 hours before measurements begin, measuring a set of standards at the
413 beginning and end of each day and every 9 samples, using Ultra High Purity (UHP) N₂ gas, and
414 filtering the N₂ gas with a PTFE filter, CO₂ scrubber (Ascarite II) and H₂O scrubber
415 (Mg(ClO₄)₂).

416 Samples were analyzed spectrophotometrically for pH with a CONTROS HydroFIA pH
417 (Abmann et al., 2011) operating in discrete measurement mode using unpurified m-Cresol Purple
418 (mCP) as the indicator dye (Clayton and Byrne, 1993). Sample temperature was stabilized at
419 25C±0.01 during measurements using Peltier elements and 5 repetitive measurements were
420 taken for each sample. At the beginning of each day, the HydroFIA pH underwent a conditioning
421 period using seawater with similar properties until values stabilized. CRMs (known TA and DIC
422 concentration, Batch #198 from A. Dickson's Certified Reference Materials Laboratory) were
423 measured at the beginning and end of the day, as well as every 9 samples.

Deleted: ¶

Deleted: are

Deleted: is

Deleted: is

Deleted: requires

Formatted: Font: (Default) Times New Roman, 12 pt, Not Bold

Deleted: is

Deleted: ¶

Deleted: UHP (

Deleted:)

433 All data ~~processing~~ and analyses were done using ~~an~~ in-house MATLAB routine. In situ
434 pH and $p\text{CO}_2^{\text{disc}}$ were calculated ~~from~~ input pair pH_{lab} and DIC using CO2SYSv3 (Sharp et al.,
435 2023) with dissociation constants for carbonic acid of Sulpis et al. (2020), bisulfate of (Dickson,
436 1990), hydrofluoric acid of Perez and Fraga, (1987), and the boron-to-chlorinity ratio of (Lee et
437 al., 2010). Sulpis et al. (2020) found that the carbonic acid dissociation constants of Lueker et al.
438 (2000) may underestimate $p\text{CO}_2$ in cold regions (below $\sim 8^\circ\text{C}$) and, therefore, overestimate pH
439 and CO_3^{2-} . Differences between discrete $p\text{CO}_2$ calculated with the carbonic acid dissociation
440 constants by Lueker et al. (2000) (the standard in synthesis data products (e.g., Jiang et al., 2021,
441 Lauvset et al., 2022, Metzl et al., 2024) and the HydroC $p\text{CO}_2$ from the tank experiment were
442 found to be on average 4.6 μatm (1.6 %) and 4.2 μatm (0.7 %) greater for SN0422 and SN0718,
443 respectively, when compared with discrete $p\text{CO}_2$ based on carbonic acid dissociation constants
444 by Sulpis et al. (2020).

Deleted: manipulation

Deleted: from

Formatted: Superscript

445 Discrete $p\text{CO}_2$ uncertainty (u_c) ~~was calculated as~~ the combined standard uncertainty from
446 *errors.m* (Orr et al., 2018) that propagates input uncertainties. Input uncertainties for pH_{lab} and
447 DIC ~~were~~ the standard uncertainties, defined as the square root of the sum of the squared random
448 uncertainty component plus the squared systematic uncertainty components. For pH_{lab} the
449 random uncertainty ~~was~~ the sample precision, or standard deviation of the measurements. For
450 DIC, the random uncertainty ~~was~~ the propagated error calculated with the first-order Taylor
451 series expansion (Equation 1, Orr et al. (2018)) and assuming the correlation term ~~was zero for~~
452 the conversion of molarity ($\mu\text{moles l}^{-1}$) to molality ($\mu\text{moles kg}^{-1}$). Systematic uncertainty
453 components ~~were~~ the uncertainty in the ~~CRM~~ used for instrument offset and drift correction, and
454 the published instrument accuracy, or if available, the daily instrument accuracy as defined
455 below. Daily instrument accuracy ~~was~~ defined as the maximum difference between the known

Deleted: is

Deleted: are

Deleted: is

Deleted: is

Deleted: is

Deleted: are

Deleted: Certified Reference Material

Deleted: is

466 CRM concentration, and the measured CRM concentration after data were corrected for
467 instrument drift and offset of all available CRM's not used in the instrument drift and offset
468 calculation. CRM pH_{lab} "known" values were calculated using CO2SYSv3 (Sharp et al., 2023)
469 with inputs pH and DIC. Nutrient concentrations (SiO₄⁻², PO₄⁻³) were assumed to be negligible in
470 the CO2SYS calculations (e.g. DeGrandpre et al., 2019; Vergara-Jara et al., 2019; Islam et al.,
471 2017).

Deleted: Certified Reference Material (
Deleted:)

Deleted: are

473 2.6.2 Methane

474 Two sets of triplicate pCH₄ discrete water samples were collected during the tank
475 experiment for an initial evaluation of the SG HydroC CH₄ sensor (Figure 4c, Table 1). Seawater
476 was filtered from the tank into 250 mL vials. The vials were closed with a rubber stopper, topped
477 with an aluminum cap, and closed with a crimp immediately. A dry and clean syringe was
478 flushed with 10 mL of N₂ gas twice. The third fill was kept, and the syringe valve was closed. N₂
479 was then injected into the headspace while simultaneously pulling 10 mL seawater out of the vial
480 using a second syringe. 50 µL mercuric chloride (HgCl₂) were added to the vial, which was then
481 shaken for about a minute and put into a fridge at 4°C for over 12 h to equilibrate the headspace.
482 The samples were then sent to the Kessler analytical laboratory at the University of Rochester for
483 analysis.

Deleted: (

Deleted:)

Deleted: (

Deleted:)

Formatted: German

Field Code Changed

Deleted: (

Deleted:)

Formatted: German

Deleted: T

Deleted: every 4 hours

Deleted: b

Deleted: straight

485 2.7 Data post-processing

486 2.7.1 pCO₂ post-processing

487 SG HydroC CO₂ data were post-processed using Jupyter Notebook scripts developed by -4H-
488 JENA engineering GmbH at the original resolution (2 seconds). SG HydroC CO₂ (SG HydroC

Deleted: notebook

Deleted: E

Deleted: 2 second

Formatted: Font: Times New Roman, 12 pt

Formatted: Font: Times New Roman

Formatted: Font: Times New Roman, 12 pt

505 CO2T-0422-001) data from the tank experiment (Table 1, Figure 4) and rosette mounted CTD
 506 casts (Table 2 and 3, Figure 7 and S1) were post-processed to correct for baseline drift (change in
 507 the zero signal reference) and span drift (changes in the sensor's concentration dependent
 508 characteristics) using pre- and post-calibration coefficients interpolated over the
 509 deployment (Fietzek et al., 2014). For the May 2022 Seaglider integrated SG HydroC
 510 CO₂ sensor (SG HydroC CO2T-0718-001, Table 3, Figures 8 and 9), data were post-processed
 511 with pre-calibration coefficients only (no span drift correction) because the sensor was damaged
 512 during the return shipment for post-calibration. Differences between sensors remained low
 513 despite the difference in processing, with a mean difference during the tank experiment of $2.1 \pm$
 514 $1.0 \mu\text{atm}$ (0.9%) and median difference of $2.0 \pm 1.0 \mu\text{atm}$ (0.9%) (Table 1, Figure 4b).
 515 The $p\text{CO}_2$ data from February 2023 was collected with a sensor that was factory calibrated two
 516 weeks prior to deployment (SG HydroC CO2T-0422-001) but were not post-processed because a
 517 required parameter (p NDIR) was not relayed in real-time and the glider was lost. Lack of post-
 518 calibration most likely had no negative effect on the quality of data since the HydroC was only
 519 collecting data for ~4 days during the spring mission and ~2 days during the winter mission.
 520 HydroC $p\text{CO}_2$ and $p\text{CO}_2^{\text{RTC}}$ data at the original resolution (2 s) and RTC resolution (8 s)
 521 were linearly interpolated onto the Seaglider timestamp and 1-meter binned data were calculated
 522 by first averaging 1 meter (+/- 0.5 m) upcast and downcast data independently, linearly
 523 interpolating over gaps, then averaging the interpolated 1-meter binned upcast and downcast
 524 together.

526 2.7.2 Response time correction

Deleted: SG HydroC CO₂ data from the
 Deleted: sensor
 Formatted: Font: Times New Roman, 12 pt

Deleted: (SG HydroC CO2T-0422-001) were post-processed using pre- and post-calibration coefficients interpolated with any change in the zero signal reference over the deployment (Fietzek et al., 2014).
 Formatted: Font: Times New Roman, 12 pt

Formatted: Font: Times New Roman, 12 pt

Formatted: Font: Times New Roman, 12 pt

Deleted: For the Seaglider integrated SG HydroC CO₂ sensor (SG HydroC CO2T-0718-001),

Formatted: Font: Times New Roman

Formatted: Font: Times New Roman, 12 pt

Formatted: Font: Times New Roman, 12 pt

Deleted:

Formatted: Font: Times New Roman, 12 pt

Formatted: Font: Times New Roman, 12 pt

Formatted: Font: Times New Roman

Formatted: Font: Times New Roman, 12 pt

Formatted: Font: Times New Roman, 12 pt

Deleted:), but

Formatted: Font: Times New Roman, 12 pt

Moved (insertion) [2]

Deleted:).

Formatted: Font: Italic

Formatted: Subscript

Formatted: Superscript

Formatted: Indent: First line: 0.5", Line spacing: Double

Deleted: ¶

Formatted: Font color: Black

Deleted: with a mean difference during the tank experiment of $2.12 \pm 0.98 \mu\text{atm}$ (0.92%) and median difference of $2.00 \pm 0.98 \mu\text{atm}$ (0.88%). The $p\text{CO}_2$ data from the February 2023 were not post-processed because a required parameter was not relayed in real-time.¶
 Formatted: Line spacing: Double

544 The ability to determine the in situ response time (τ_{63} of the HydroC, which took into
 545 account membrane characteristics and the rate of water exchange over the membrane, i.e.
 546 pump characteristics) of the sensor made correction for hysteresis through data post processing
 547 possible. This is critical for a sensor operating on profiling platforms, especially in the Gulf of
 548 Alaska, where strong environmental gradients were encountered. Fiedler et al. (2013) used a
 549 CONTROS HydroC™ CO₂ with a silicone, polydimethylsiloxane (PDMS) membrane and
 550 reported a linear response time dependency on water temperature on the order of one second per
 551 one °C. For this study, the SG HydroC CO₂ sensors were deployed with the new robust TOUGH
 552 membrane, which had Teflon AF2400 as the active separation layer with a low temperature
 553 dependence on the permeability coefficient (Pinnau and Toy, 1996). Response times determined
 554 during calibration at -4H-JENA were used for response time correction (RTC) and found to be
 555 106 seconds for the HydroC mounted on the rosette in May 2022 and 108 seconds when it was
 556 integrated into the Seaglider in February 2023 (HydroC CO2T-0422-001). The response time of
 557 the HydroC integrated into the Seaglider in May 2022 (HydroC CO2T-0718-001) was 109
 558 seconds. Since field verification of the response time was recommended to ensure the highest
 559 quality post-processed data product (because τ_{63} can be affected by the speed of water exchange
 560 across the membrane (e.g. pump speed, tube length, etc.)), we verified the sensor response time
 561 at deployment. After the glider was stationary for approximately 15 minutes, a zeroing interval
 562 was performed with the HydroC CO₂. The response time was determined by reviewing the time
 563 it took for the signal to recover to the ambient concentration. Our in situ response time tests were
 564 suggested to be within 5 seconds of the response time found during calibration (not shown).
 565 Before RTC was applied, HydroC CO₂ data were smoothed using a quadratic regression
 566 (MATLAB's smoothdata.m function with the loess method) over a 2-minute window. This was

- Deleted: t_
- Deleted: 63
- Formatted: Font color: Auto
- Formatted: Font color: Auto
- Formatted: Font color: Auto, Subscript
- Formatted: Indent: First line: 0.5", Line spacing: Double
- Deleted: enables
- Deleted: the user to
- Deleted: ,
- Deleted: or anywhere
- Deleted:
- Deleted: are
- Formatted: Font: Not Italic
- Deleted: -1 s per
- Deleted: 1
- Deleted: uses
- Deleted: and which has
- Deleted:), so no temperature dependency on our sensor's response times were observed
- Deleted: The response time with the HydroC CO₂ TOUGH membrane is very generally stable but can be affected (... [1])
- Formatted: Font: (Default) Times New Roman, Not Italic
- Moved (insertion) [1]
- Deleted: Response times were determined during calit... [2]
- Deleted: Since
- Deleted: f
- Deleted: F
- Deleted: is
- Deleted:
- Deleted: .
- Deleted: . Our in situ response time tests suggest to be (... [3])
- Deleted: pCO₂ concentrations are stable by performing a
- Deleted: and
- Deleted: takes
- Deleted: ¶
- Formatted: Font: (Default) Times New Roman, Not Italic
- Formatted (... [4])
- Formatted: Font: (Default) Times New Roman, Not Italic
- Deleted: 2 minute
- Formatted: Font: (Default) Times New Roman, Not Italic

613 done to eliminate erroneous spikes in the RTC signal while retaining the original 2-second
 614 resolution of the $p\text{CO}_2$ data. The RTC resolution of 8 seconds was determined with the L-curve
 615 analysis included in the publicly available code from Dølven et al. (2022). The Dølven et al.
 616 (2022) RTC method was used because it produced more realistic profiles than an RTC method
 617 (Miloshevich et al., 2004, not shown) previously used for HydroC CO_2 correction from a
 618 profiling float (Fielder et al. 2013). In addition, Dølven et al. (2022) developed their algorithm
 619 with equilibrium-based sensors in mind and was proven with a sensor with a long response time
 620 (HydroC CH_4 $\tau_{63} \approx 23$ minutes).

622 2.7.3 $p\text{CH}_4$ post-processing

623 SG HydroC $p\text{CH}_4$ data were response time corrected using a τ_{63} of 43 minutes (Dølven et
 624 al., 2022; Figure 4c, blue line). Before RTC was applied, HydroC CH_4 data were smoothed using
 625 a quadratic regression (MATLAB's smoothdata.m function with the L_{ess} method) over a 2-
 626 minute window to avoid erroneous spikes in the RTC data while retaining the original 2-second
 627 resolution of the $p\text{CH}_4$ data. The RTC resolution of 30 seconds was determined with the L-curve
 628 analysis included in the publicly available code from Dølven et al. (2022). Discrete CH_4 samples
 629 were collected during the tank experiment (Table 1; Figure 4c red diamonds) and analyzed at
 630 John Kessler's laboratory at the University of Rochester. Discrete CH_4 sample values were
 631 converted from the concentration of dissolved gas in water (mol L^{-1}) to partial pressure ($p\text{CH}_4^{\text{disc}}$,
 632 μatm) using the solubility coefficient following Sarmiento and Gruber (2006). $p\text{CH}_4^{\text{disc}}$
 633 uncertainty (u ; Table 1; Figure 4c red error bars) was calculated as the square root of the sum of
 634 the squared 1) mean of the standard deviations from each sample as returned from the lab and 2)
 635 the standard deviation of the triplicates.

Deleted: data

Deleted: and

Deleted:

Formatted: Font: (Default) Times New Roman, Not Italic

Formatted ... [5]

Formatted: Font: (Default) Times New Roman, Not Italic

Formatted: Font: (Default) Times New Roman

Formatted ... [6]

Formatted: Font: Times New Roman, 12 pt, Subscript

Formatted: Font: Times New Roman, 12 pt

Deleted: , so we opted to use the Dølven et al. (2022) algorithm

Moved up [2]:). HydroC data at the original resolution (2 s) and RTC resolution (8 s) were linearly interpolated onto the Seaglider timestamp and 1-meter binned data were calculated by first averaging 1 meter (+/- 0.5 m) upcast and downcast data independently, linearly interpolating over gaps, then averaging the interpolated 1-meter binned upcast and downcast together.

Formatted ... [7]

Formatted ... [8]

Moved up [1]: Response times were determined during calibration at 4H-JENA and found to be 106 and 108 seconds for HydroC CO2T-0422-001 when mounted on the rosette in May 2022 and when integrated onto the Seaglider in February 2023, respectively. The response time of the sensor integrated into the Seaglider in May 2022 (HydroC CO2T-0718-001) was 109 seconds. A one-minute average was taken before response time correction was applied. Response time correction (RTC) was applied with 60 second resolution using the publicly available code from Dølven et al. (2022). There was no major difference (not shown) in RTC $p\text{CO}_2$ between the Dølven et al. (2022) and an RTC method (Miloshevich et al., 2004) previously used for HydroC CO_2 correction from a profiling float (Fielder et al. 2013), so we opted to use the Dølven et al. (2022) algorithm since it was developed with equilibrium-based sensors in

Deleted: Response times were determined during calit... [9]

Deleted: τ_{63}

Formatted ... [10]

Formatted: Indent: First line: 0.5", Line spacing: Double

Formatted ... [11]

Deleted: L...ess method) over a 2-minute window to ... [12]

Formatted: Font: Italic

Formatted ... [13]

Formatted ... [14]

Formatted ... [15]

Formatted: Font color: Black

746

747 3. Results

748 3.1 Glider flight

749 Despite the large payload and major changes to the vehicle fairing, the glider was able to
 750 “fly” properly, allowing the desired undisturbed flow to meet the sensor's requirements. Example
 751 flight profiles with the POM and Titanium integrated sensors are shown in Figures 5 and 6,
 752 respectively. Pitch and vertical velocity are in the stable range, and roughly symmetric between
 753 downcast and upcast, indicating a nearly balanced glider. Heading varies around the targeted
 754 value as the roll adjusted to heading errors. It should be noted that this level of variability is
 755 typical of standard Seagliders. Operating Seagliders in shallow water (<200 m) is risky because
 756 of the likelihood of meeting depth-averaged currents of the same order of magnitude as the
 757 vehicle speed. A typical single dive cycle of downcast and upcast shows that the sensor data are
 758 free of noise that could be expected if there were recirculated water from the glider meeting the
 759 sensors. The expected endurance of the CO₂ Seaglider is around 18 days and 15 days for the
 760 CH₄ Seaglider with constant sampling at full depth.

761

762 3.2 CO₂ Seaglider data evaluation

763 The quality of the CO₂ Seaglider data was thoroughly tested with discrete measurements
 764 during a tank experiment, nearby CTD cast, and glider missions.

765

766 3.2.1 Tank experiment

767 Discrete water samples show good agreement with the SG HydroC CO₂ sensors (Figure
 768 4b, Table 1). The values of discrete water samples represent the average of triplicate samples

Deleted: For the best possible accuracy, HydroC CH₄ sensors should be returned to -4H-JENA engineering GmbH for a post deployment performance verification. This includes a response time verification in the calibration tank at the pre-deployment verification conditions, as well as at the water temperature found in the field covering typical pCH₄ changes. A verification of the detector stability using reference gases with an accuracy of 0.5% can be provided. A response time of ~25 minutes was found with a 5T pump (Seabird Electronics) and found to be ~1.7 times slower with a 5M pump (Seabird Electronics). Response time correction was applied using a response time of ~43 minutes and the publicly available code from Dolven et al. (2022) (Figure 4b).

Formatted: Highlight

Deleted: from the

Deleted: 300 m and 1000 m configurations

Deleted: and underway

Deleted: CO₂ Seaglider data

Deleted: 4a

788 (Figure 4c, red diamonds). Differences between the SG HydroC CO₂ sensors remained low, with
 789 a mean difference during the tank experiment of 2.1 ± 1.0 μatm (0.9%) and median difference of
 790 2.0 μatm (0.9%; Table 1). Percent differences (Eq. 1) between the SG HydroC CO₂ sensors and
 791 discrete water samples collected in the tank were between 0.3 and 1.9% (Table 1, Figure 4).

792
$$\% \text{ difference} = \frac{pCO_2^{HydroC} - pCO_2^{disc}}{(pCO_2^{HydroC} + pCO_2^{disc})} / 2 * 100\%$$
 (Equation 1)

794 3.2.2 Profiling experiment

795 Rosette-based profiles with the SG HydroC CO₂ sensor in combination with discrete
 796 water samples were used to test and evaluate the response correction algorithm by Dølven et al.

797 (2022). The rosette was lowered into the water and kept at different depths for about 20 minutes
 798 at a time (Figure 7a and Figure S1a). Sample bottles were programmed to collect seawater
 799 toward the end of each hovering period. pCO₂ measured with the HydroC ranged from 218 μatm
 800 at the surface to 411 μatm at 80 m depth on May 3 (Figure 7b) and 231 μatm at the surface to
 801 382 μatm at 77 m depth on May 7 (Figure S1). Differences between the rosette mounted SG
 802 HydroC CO₂ sensor and discrete samples ranged from -3.3 μatm (1.4%) to 8.2 μatm (3.4%)
 803 with a lowest percent difference of 0.6% (Table 2) on May 3 and from -5.7 μatm (1.6%) to 12.1
 804 μatm (3.8%) with a lowest percent difference of 0.3% (Table 3) on May 7.

806 3.2.3 Data evaluation during CO₂ Seaglider mission

807 The quality of the pCO₂ data from the CO₂ Seaglider was further evaluated during a 3-
 808 day long sea trial mission in spring 2022 in Resurrection Bay, Alaska (Figure 3).

- Deleted: 4a
- Deleted: dots
- Deleted: 2
- Deleted: 0.98
- Deleted: 1
- Deleted: 0
- Deleted: 88
- Deleted: ,
- Deleted: 2
- Deleted: 7

- Deleted: 5m, 20m, 40m, 60m and 80m

- Deleted:

- Deleted: 9

- Deleted: 409

- Deleted: 2.3
- Deleted: 0.9
- Deleted: 9.3
- Deleted: 4.2
- Deleted: .
- Deleted: ¶
- Deleted: ¶

830 Discrete water samples were taken in proximity (1 km and within 4 hours) of the downcast of
 831 dive #51 (Figures 8 and 9a, Table 3). The response time corrected CO₂ Seaglider data compares
 832 well with the discrete water samples (Figure 8), overestimating the discrete water samples
 833 between 8.3 μatm (2.6 %) and 12.0 μatm (5.0 %) (Table 3). The mean difference between the
 834 rosette mounted and Seaglider integrated SG HydroC CO₂ sensors during the May 7th cast at the
 835 time of discrete samples was 8.5 μatm +/- 8.9 μatm (3.7 %). The larger difference between SG
 836 HydroC CO₂ sensors compared to the difference during the tank experiment (see Section 3.2.1)
 837 is unsurprising, given the spatial and temporal distance between sensors (Table 3). Collecting
 838 more discrete samples throughout the water column and in closer proximity (within 100 m,
 839 Thompson et al., 2021) to the CO₂ Seaglider conducting dives would allow a more tightly
 840 constrained uncertainty estimate for response time corrected pCO₂ data collected on a glider and
 841 should be a priority for future researchers.

Deleted: 500
 Deleted: and within 30 - 60 minutes

Deleted: , dash
 Deleted: ed black line
 Deleted: 6.6
 Deleted: 1
 Deleted: 15.1
 Deleted: 6.3

Formatted: Subscript

Formatted: Subscript

Commented [B13]: Claudine I added this, what do you think?
 Formatted: Font: Bold

843 3.3 CH₄ Seaglider data evaluation

844 3.3.1 Tank experiment

845 The SG HydroC CH₄ was also evaluated during the tank experiment described in section
 846 2.4 (Figure 4c). Percent differences (Eq. 1) between discrete pCH₄ (average of triplicate samples)
 847 and pCH₄^{RTC} were 6.3 to 14.6 % (Table 1). During the experiment, there was a decrease in
 848 salinity from 30.95 to 29.88 where pCO₂ decreased by 80 μatm. The corresponding pCH₄^{RTC}
 849 signal decreased by 25.4 μatm from 32.3 to 6.9 μatm. Although the triplicate discrete pCH₄ water
 850 samples were slightly lower than the sensor-measured pCH₄ values, they also reflected this step
 851 change.

Deleted: Relative
 Formatted: Font: (Default) Times New Roman, 12 pt
 Formatted: Font: (Default) Times New Roman, 12 pt

Deleted: correspondingly
 Formatted: Font: (Default) Times New Roman, 12 pt, Subscript
 Formatted: Font: (Default) Times New Roman, 12 pt

Deleted: During the experiment there was a decrease in salinity from 30.95 to 29.88 and pCO₂ correspondingly decreased by 83 μatm. The corresponding pCH₄ RTC signal decreased from 31.8 μatm to 6.6 μatm.

Deleted: sensor
 Formatted: Font color: Black

868 **3.4 Winter and springtime pCO₂ in Resurrection Bay, Alaska**

869 The surface-to-subsurface pCO₂ gradient is much larger in spring than in winter (Figure
870 10). During the early May mission, the average surface pCO_{2,Seaglider^{RTC}} was 240.7 +/- 16.5 μatm
871 (mean +/- standard deviation at 2 meters), with an average temperature of 5.8 +/- 0.4 °C (Figures
872 9 and 10). In February, surface pCO_{2,Seaglider^{RTC}} was near atmospheric pCO₂ (427.4 +/- 13.0 μatm,
873 temperature 4.1 +/- 0.3 °C) and about 180 μatm higher than in May (Figures 10 and 11).
874 NOAA's moored sensor located in Sunny Cove (59.911 °N, -149.35 °W), near the CO₂ Seaglider
875 trial site, measured an average sea surface pCO₂ of 240.7 +/- 10.4 μatm during the time of the
876 May 2022 mission (Monacci et al., 2023), which compared remarkably well with the Seaglider
877 based measurements. A minimum of 140 μatm was measured in Sunny Cove in mid-April (3-day
878 average) (Figure 12, Monacci et al., 2023), suggesting that the peak of the spring bloom
879 happened three weeks before the May 2022 glider mission. Since we don't have salinity data
880 from the May CO₂ Seaglider mission (conductivity sensor failure), we cannot disentangle the
881 contributions of freshwater or primary production on the low surface pCO₂ values observed.
882 (Figure 9). The moored sensor in Sunny Cove measured an average sea surface pCO₂ of 416.4
883 +/- 4.2 μatm during the time of the February mission, straddling the atmospheric pCO₂ values
884 (Monacci et al., 2023, Figure 12). Subsurface pCO_{2,Seaglider^{RTC}} at 180 m was on average 545.6 +/-
885 16.9 μatm during the February mission and 518.2 +/- 37.4 μatm during the May 2022 mission
886 (Figure 10a). pCO₂ was much lower in May than in February throughout the upper water column
887 (<120 m), whereas there was not much of a seasonal difference at deeper depth. Some of the
888 fine scale features apparent in the May pCO₂ and O₂ profiles are likely due to various levels of
889 photosynthetic activity (Figure 10). As the glider transitioned into the open Gulf of Alaska
890 during the February mission, water with O₂ < 150 μM shoaled into the upper 150 m of the water

- Deleted: to
- Deleted: pCO₂
- Deleted: 240.8
- Deleted: 17.6
- Commented [B14]: I changed values from 1 meter to 2 meter to limit influence of RTC/increase number of points to average
- Deleted: 1
- Deleted:
- Deleted: 9
- Deleted:
- Deleted: 420
- Deleted: .
- Deleted: 5
- Deleted: 11.3
- Deleted: 0
- Formatted: Font: Not Bold
- Deleted:
- Formatted: Font: Not Bold
- Formatted: Font: Not Bold
- Deleted: s
- Formatted: Font: Not Bold
- Formatted: Font: Not Bold
- Deleted: prior to
- Deleted: our
- Deleted: As a comparison, NOAA's moored sensor located in Sunny Cove (59.911 °N, -149.35 °W), near the CO₂ Seaglider trial site, measured an average surface pCO₂ of 240.7 +/- 10.4 μatm during the time of the May 2022 mission and a minimum of 140 μatm in mid-April (3-day average) (Figure 12, Monacci et al., 2023), suggesting that the peak of the spring bloom happened three weeks prior to our glider mission....
- Formatted: Font: Not Bold
- Formatted: Font: Not Bold
- Deleted: that were
- Deleted: during the May mission
- Deleted: pCO₂
- Deleted: 6
- Deleted: 8
- Deleted: 0
- Deleted: 16.3
- Deleted: 2.7

924 column (Figure 11). Unfortunately, the HydroC CO₂ sensor was turned off at that stage of the
925 mission to conserve battery.

926

927 4. Discussion

928 The newly developed CO₂ Seaglider is the first of its kind to autonomously collect high
929 quality pCO₂ data. The tank and rosette experiments and in situ data evaluation suggest that the
930 post-processed data from the CO₂ Seaglider generally fall near the relative uncertainty of 2.5%,
931 which is a threshold defined as the “quality sufficient to identify relative spatial patterns and
932 short-term variation” (“weather quality”, Newton et al., 2015). This is the highest quality of
933 pCO₂ data that has been measured with a subsurface autonomous vehicle to this date and

934 therefore an important step towards filling the subsurface carbonate system data gap, -4H-JENA,
935 is reassessing their sensor calibration methodology and data post-processing algorithm to further
936 improve the HydroC’s data accuracy.

937 The newly developed CO₂ Seaglider is suitable for data collection in open ocean or
938 coastal environments with bottom depths deeper than 300 m. However, the coastal Gulf of
939 Alaska is a highly dynamic environment, with strong freshwater and wind influence, and rugged
940 shallow (often < 200 m) bottom topography. Strong currents (up to 0.50 m s⁻¹) made the piloting
941 of the glider extremely difficult throughout the project and confirmed that the Seaglider cannot
942 reliably reach desired waypoints in these conditions. The current version of the CO₂ Seaglider is
943 also not suitable for operating in the coastal Gulf of Alaska in summer and early fall, due to
944 strong seasonal salinity gradients in this freshwater influenced area. Another issue we faced was
945 the fact that the forward-looking altimeter could not detect the Seafloor as it should in its
946 position behind the HydroC CO₂. In areas with detailed topography maps this would not be an

Deleted: down to 1000 m depth

Deleted: pCO₂

Deleted: in glider accessible regions

Deleted: ena

Formatted: Font: Not Italic

Formatted: Not Highlight

Deleted: Another issue we faced was the fact that the transducer did not work in its position behind the HydroC CO₂.

954 issue, but in the coastal Gulf of Alaska reliable topography information is not readily available
955 yet. An obvious next step is to integrate the SG HydroC CO₂ sensor into a newer glider platform,
956 such as the Seaglider SGX or Teledyne Slocum G3 glider. The extended energy bay, larger
957 buoyancy range, and thruster should make the operation of the coastal Slocum G3 with HydroC
958 sensors relatively easy and would allow for autonomous high-resolution water column
959 measurements of *p*CO₂ and *p*CH₄ in dynamic coastal environments. The integration of a HydroC
960 on a Slocum glider will require a custom-made wet-payload bay due to the size of this sensor.
961 For open ocean or deeper coastal regions, the integration with the Seaglider SGX, with 60%
962 higher energy capacity, would be effective and nearly identical to the work already done here.

963 The SG HydroC CH₄ was successfully integrated into the Seaglider as part of this project.
964 While tank experiments showed promising results, short field tests of the CH₄ Seaglider in
965 shallow water revealed low and patchy methane concentrations near the detection limit (not
966 shown). The CH₄ Seaglider requires further testing in environments with strong *p*CH₄ gradients
967 during longer and deeper dives (to allow for equilibration) to assess the accuracy of its
968 response time-corrected data in the field. The sensor's slow response time likely limits the glider
969 to providing qualitative rather than quantitative results. However, due to the scarcity of oceanic
970 CH₄ observations, deploying a CH₄ glider can help identify the location of methane sources and
971 guide the placement of in situ observations to conduct a more quantitative assessment of CH₄
972 fluxes and dynamics.

973 Ocean gliders are part of the Intergovernmental Oceanographic Commission (IOC-
974 UNESCO) Global Ocean Observing System (GOOS) through the OceanGliders program
975 (<https://www.oceangliders.org/>). Like other elements of the GOOS coordinated by OceanOPs of
976 the Observation Coordination Group (floats, buoys, moorings, ships, and tide gauges),

Formatted: Line spacing: Double

Formatted: Indent: First line: 0", Line spacing: Double

Formatted: Font: Italic

Formatted: Subscript

Deleted: While the results from our initial tank experiments look promising, the CH₄ Seaglider still needs to be thoroughly tested in an environment with strong *p*CH₄ gradients to fully evaluate the glider-based *p*CH₄ response time corrected data. -4-H JENA is currently developing a combined HydroC CH₄/CO₂ sensor with the same form factor as the current HydroC CO₂ and CH₄ sensors, which will make integration into the Seaglider or other platforms relatively simple and open new opportunities to monitor both gases at the same time.

Formatted: Font color: Black

987 OceanGliders contributes to “Ocean Observation for Climate, Ocean Health and Real Time
988 Services”. CO₂ gliders are perfectly suited to contribute data for understanding relevant
989 inorganic carbon processes in coastal shelf and boundary regions where mesoscale or sub-
990 mesoscale variability dominates. The current work can also serve as a first step to bring together
991 interested scientists and engineers to further develop and improve the capability of gliders to
992 measure high-quality data. OceanGliders supports this effort by promoting the formation of
993 volunteer international task teams, for which a task team could be requested for oceanographic
994 greenhouse gas research. By doing this, the visibility and availability of data will be improved as
995 well, since GOOS provides an interactive data platform for all its programs ([https://www.ocean-](https://www.ocean-ops.org/board)
996 [ops.org/board](https://www.ocean-ops.org/board)). An OceanGliders task team could also be linked with the GOOS-sponsored
997 Global Climate Observing System (GCOS: <https://gcos.wmo.int/en/home>) program through their
998 Ocean Observations Physics and Climate Panel (OOPC): “a scientific expert advisory group
999 charged with making recommendations for a sustained global ocean observing system for
1000 climate.”

Formatted: Font: Not Bold

Deleted: s

Deleted: CO₂ and CH₄ gliders are perfectly suited to contribute data related to the respective global cycles of those compounds, for understanding relevant processes in coastal shelf and boundary regions where mesoscale or sub-mesoscales dominate.

Formatted: Font: Not Bold

Formatted: Font: Not Bold

Deleted: high

Deleted: through

1001

1002 5. Concluding Thoughts

1003 Near real-time and high-resolution water column data that can be retrieved from gliders
1004 outfitted with sensors measuring salinity, temperature, inorganic carbon system parameters,
1005 oxygen, and $p\text{CH}_4$ are key to tackling a variety of today’s climate change-related issues. These
1006 datasets will become instrumental in advancing biogeochemical model forecasting and early
1007 warning systems for extreme heat, acidity, and oxygen compound events that affect coastal
1008 subsistence communities, commercial fisheries, and mariculture. Furthermore, using
1009 biogeochemical gliders to monitor the environment of tagged organisms (e.g. crabs, fish) would

Deleted: real

Deleted: e

Deleted: change

Deleted: to advance

1022 provide insight into the organism's position and behavior relative to important environmental
1023 drivers across susceptible ecosystems. Such biogeochemical glider data will help bridge in situ
1024 chemical and biological measurements, and environmental change to impacts on biology, and
1025 thereby fill an important research gap (Widdicomb et al., 2023). Potentially large natural and
1026 anthropogenic sources of CH₄ may become contributors to climate change, and if oxidized, to
1027 ocean acidification (Garcia-Tigreros et al., 2021; Sparrow et al., 2018; Shakhova et al., 2010;
1028 Rees et al., 2022). These CH₄ sources need to be properly assessed, and quantified, and if
1029 characterized as anthropogenic origin, emitters must be held accountable (Goodman et al., 2022).
1030 Once the combined HydroC CH₄/CO₂ is available it will provide a new tool to co-measure pCH₄
1031 and pCO₂ and give valuable insight into these processes and feedback mechanisms. Other
1032 advancing fields, such as marine Carbon Dioxide Removal (mCDR) and monitoring,
1033 verification, and reporting (MRV) thereof will also need detailed knowledge of the distribution
1034 of CO₂ in the water column (National Academies of Sciences, Engineering, and Medicine.
1035 2022).

1036 The CO₂ Seaglider has been extensively tested and is ready to be used in open ocean
1037 environments. An important next step will be to integrate the HydroC CO₂ and CH₄ sensors into
1038 a glider platform that reliably functions in shallow, and freshwater-affected coastal areas, such as
1039 the Gulf of Alaska, to be able to fill the large spatial and temporal data gap in these highly
1040 dynamic areas.

1042 Data availability

1043 The CO₂ Seaglider data is publicly available (Hauri et al., 2022; 2023). The HydroC,
1044 specific SIRMA code and CNF file are available on Github (Cyprus-Subsea, 2024a and 2024b).

Deleted: ,

Deleted: of

Deleted: freshwater

Deleted: glider

Deleted: CITE

Deleted: The data is currently being prepared for publication on Pangaea.de.

Deleted:

Formatted: Subscript

Formatted: Not Highlight

Formatted: Indent: First line: 0.5"

Deleted: is

Deleted:) and the CNF file is available as supplemental material...

1056 More detailed information on the HydroC – glider integration and operation can be found in the
1057 CO₂ Seaglider Standard Operating Procedures (Irving et al., 2024).

- Deleted: OceanGliders
- Deleted: [https://github.com/britairving/Carbon_Dioxide_SO P...](https://github.com/britairving/Carbon_Dioxide_SO_P...)
- Deleted: CITE
- Formatted: Subscript

1059 Author contributions

1060 C.H. and A.M. developed the research ideas and the proposal that funded this work. C.H.
1061 led the fieldwork and writing of this manuscript. B.I. led the preparation for fieldwork and glider
1062 data processing and analysis. D.H. led glider piloting for all trials. D.H. and E.A. assisted with
1063 data processing, sensor programming, mechanical integration, glider ballasting, deployment, and
1064 recovery. N.K. and J.K. provided technical support for the HydroC sensors. All authors
1065 contributed to the writing of this manuscript.

1067 Competing interests

1068 Authors Hayes and Abdi are employed by AOOI and CSCS (respectively) and their
1069 objective is to support the ocean research community by providing innovative, cutting-edge
1070 observing technological solutions. These include autonomous platforms and related services in
1071 unique configurations. Through the support of the National Science Foundation and the National
1072 Oceanographic Partnership Program, AOOI was able to jointly develop the CO₂ and CH₄ gliders
1073 and prove and improve the scientific utility of this approach. Authors Kinski and Kemme are
1074 employed by -4H-JENA engineering GmbH, the manufacturer of the HydroC CO₂ and CH₄
1075 sensors. The objective of -4H-JENA engineering GmbH is to provide best possible accuracy of
1076 dissolved gas measurements on any platform and at any environmental condition. Intensive
1077 collaboration with scientists is essential for the development of these products.

- Formatted: Font: (Default) Times New Roman, 12 pt, Not Bold
- Formatted: Indent: First line: 0.5", Line spacing: Double
- Formatted: Font: (Default) Times New Roman, 12 pt, Not Bold, Subscript
- Formatted: Font: (Default) Times New Roman, 12 pt, Not Bold
- Formatted: Font: (Default) Times New Roman, 12 pt, Not Bold, Subscript
- Formatted: Font: (Default) Times New Roman, 12 pt, Not Bold
- Formatted: Font: (Default) Times New Roman, 12 pt, Not Bold, Subscript
- Formatted: Font: (Default) Times New Roman, 12 pt, Not Bold
- Formatted: Font: (Default) Times New Roman, 12 pt, Not Bold
- Formatted: Font: (Default) Times New Roman, 12 pt, Not Bold
- Deleted: The authors have no competing interests.¶

1084 **Acknowledgments**

1085 The Seaglider field trials took place in the traditional and contemporary hunting grounds
1086 of the Sugpiaq People. We also acknowledge that our Fairbanks-based offices are located on the
1087 Native lands of the Lower Tanana Dena. The Indigenous Peoples never surrendered lands or
1088 resources to Russia or the United States. We acknowledge this not only because we are grateful
1089 to the Indigenous communities who have been in deep connection with the land and water for
1090 time immemorial, but also in recognition of the historical and ongoing legacy of colonialism. We
1091 are committed to improving our scientific approaches and working towards co-production for a
1092 better future for everyone.

1093 We would like to thank Jack Triest for his technical support throughout the project. We
1094 are also grateful to Brian Mullaly, Captain of the RV Nanuq, and Seward Marine Center staff,
1095 especially Pete Shipton, Ed DeCastro, Jenny Grischuk, and Jenny Elhard for their assistance
1096 during the field trials in Seward. We are also grateful for the support from the Alutiiq Pride
1097 Marine Institute, Alaska Sealife Center, and the Autonomous Remote Technology Lab. Finally,
1098 we would like to express our gratitude to John Kessler and Katherine Gregory for analyzing our
1099 CH₄ discrete water samples, guiding us through the sampling process and discussing CH₄
1100 Seaglider missions with us. We would also like to thank for the support of Cyprus Subsea
1101 engineers Sergey Vekli, Loizos Groutas, and Jerald Reodica in mechanical and electronic sensor
1102 integration and piloting, as well as assisting with Cyprus sea testing of the HydroC sensors and
1103 CO₂ Seaglider.

1104

1105 **Financial support**

1106 We would like to thank the National Oceanographic Partnership Program and the
1107 National Science Foundation for the support of this project (OCE-1841948).

1108 **References**

1109 Aßmann, S., Frank, C., and Körtzinger, A.: Spectrophotometric high-precision seawater pH
1110 determination for use in underway measuring systems, *Ocean Sci.*, 7, 597–607,

1111 <https://doi.org/10.5194/os-7-597-2011>, 2011.

1112

1113 [Barnes, R. O. and Goldberg, E. D. Methane production and consumption in anoxic marine](#)
1114 [sediments. *Geology* 4, 297–300, 1976.](#)

1115

1116 Bittig, H. C., Körtzinger, A., Neill, C., van Ooijen, E., Plant, J. N., Hahn, J., Johnson, K. S.,

1117 Yang, B., and Emerson, S. R.: Oxygen Optode Sensors: Principle, Characterization, Calibration,

1118 and Application in the Ocean, *Front. Mar. Sci.*, 4, <https://doi.org/10.3389/fmars.2017.00429>,

1119 2018.

1120

1121 Bockmon, E. E. and Dickson, A. G.: A seawater filtration method suitable for total dissolved

1122 inorganic carbon and pH analyses, *Limnology and Oceanography Methods*, 12(4), 191–195,

1123 <https://doi.org/10.4319/lom.2014.12.191>, 2014.

1124

1125 Breitberg, D., Salisbury, J., Bernhard, J., Cai, W.-J., Dupont, S., Doney, S., Kroeker, K., Levin,

1126 L., Long, W. C., Milke, L., Miller, S., Phelan, B., Passow, U., Seibel, B., Todgham, A., and

1127 Tarrant, A.: And on Top of All That... Coping with Ocean Acidification in the Midst of Many

1128 Stressors, *Oceanography*, 25, 48–61, <https://doi.org/10.5670/oceanog.2015.31>, 2015.

1129

1130 Breitburg, D., Levin, L. A., Oschlies, A., Grégoire, M., Chavez, F. P., Conley, D. J., Garçon, V.,

Formatted: Widow/Orphan control, Border: Top: (No border), Bottom: (No border), Left: (No border), Right: (No border), Between : (No border)

1131 Gilbert, D., Gutiérrez, D., Isensee, K., Jacinto, G. S., Limburg, K. E., Montes, I., Naqvi, S. W.
1132 A., Pitcher, G. C., Rabalais, N. N., Roman, M. R., Rose, K. A., Seibel, B. A., Telszewski, M.,
1133 Yasuhara, M., and Zhang, J.: Declining oxygen in the global ocean and coastal waters, *Science*,
1134 359, 46, <https://doi.org/10.1126/science.aam7240>, 2018.

1135

1136 Briggs, E. M., Martz, T. R., Talley, L. D., Mazloff, M. R., and Johnson, K. S.: Physical and
1137 Biological Drivers of Biogeochemical Tracers Within the Seasonal Sea Ice Zone of the Southern
1138 Ocean From Profiling Floats, *J. Geophys. Res. Oceans*, 123, 746–758,
1139 <https://doi.org/10.1002/2017JC012846>, 2018.

1140

1141 Chavez, F. P., Sevadjan, J., Wahl, C., Friederich, J., and Friederich, G. E.: Measurements of
1142 $p\text{CO}_2$ and pH from an autonomous surface vehicle in a coastal upwelling system, *Deep Sea Res.*
1143 *Part II Top. Stud. Oceanogr.*, 151, 137–146, <https://doi.org/10.1016/j.dsr2.2017.01.001>, 2018.

1144

1145 Claustre, H., Johnson, K. S., and Takeshita, Y.: Observing the Global Ocean with
1146 Biogeochemical-Argo, *Annu. Rev. Mar. Sci.*, 12, 23–48, [https://doi.org/10.1146/annurev-](https://doi.org/10.1146/annurev-marine-010419-010956)
1147 [marine-010419-010956](https://doi.org/10.1146/annurev-marine-010419-010956), 2020.

1148

1149 Clayton, T. D. and Byrne, R. H.: Spectrophotometric seawater pH measurements: total hydrogen
1150 ion concentration scale calibration of m-cresol purple and at-sea results, *Deep Sea Res. Part*
1151 *Oceanogr. Res. Pap.*, 40(10), 2115–2129, 1993.

1152

1153 [Cyprus-Subsea; Smart-Cable-HydroC. GitHub repository \[code\]](#), [https://github.com/Cyprus-](https://github.com/Cyprus-Subsea/Smart-Cable-HydroC)

Deleted: .

Formatted: Font: (Default) Times New Roman, 12 pt

Formatted: Font: (Default) Times New Roman, 12 pt

1155 [Subsea/Smart-Cable-HydroC](#) (last access: 14 June 2024), 2024a.

1156

1157 [Cyprus-Subsea: CO₂ and CH₄ CNF files, GitHub repository \[code\]](#), [https://github.com/Cyprus-](https://github.com/Cyprus-Subsea/Smart-Cable-HydroC/tree/main/docs)

1158 [Subsea/Smart-Cable-HydroC/tree/main/docs](#) (last access: 7 July 2024), 2024b.

1159

1160 DeGrandpre, M. D., Lai, C. Z., Timmermans, M. L., Krishfield, R. A., Proshutinsky, A., and

1161 Torres, D.: Inorganic Carbon and *p*CO₂ Variability During Ice Formation in the Beaufort Gyre of

1162 the Canada Basin, *J. Geophys. Res. Oceans*, 124, 4017–4028,

1163 <https://doi.org/10.1029/2019JC015109>, 2019.

1164

1165 Dickson, A. G.: Thermodynamics of the dissociation of boric acid in synthetic seawater from

1166 273.15 to 318.15 K, *Deep Sea Res. Part Oceanogr. Res. Pap.*, 37, 755–766,

1167 [https://doi.org/10.1016/0198-0149\(90\)90004-F](https://doi.org/10.1016/0198-0149(90)90004-F), 1990.

1168

1169 Dickson, A. G. G., Sabine, C. L., Christian J.R., Christian, J. R., and Christian J.R.: Guide to

1170 Best Practices for Ocean CO₂ Measurements, *PICES Spec. Publ.* 3, 191, 2007.

1171

1172 Dølven, K. O., Vierinen, J., Grilli, R., Triest, J., and Ferré, B.: Response time correction of slow-

1173 response sensor data by deconvolution of the growth-law equation, *Geosci. Instrum. Methods*

1174 *Data Syst.*, 11, 293–306, <https://doi.org/10.5194/gi-11-293-2022>, 2022.

1175

1176 Doney, S. C., Fabry, V. J., Feely, R. A., and Kleypas, J. A.: Ocean Acidification: The Other CO₂

1177 Problem, *Annu. Rev. Mar. Sci.*, 1, 169–192,

Deleted: ly

Formatted: Font: (Default) Times New Roman, 12 pt

Formatted: Font: (Default) Times New Roman, 12 pt, Subscript

Formatted: Font: (Default) Times New Roman, 12 pt

Formatted: Font: (Default) Times New Roman, 12 pt, Subscript

Formatted: Font: (Default) Times New Roman, 12 pt

Formatted: Font: (Default) Times New Roman, 12 pt, Not Highlight

Formatted: Font: (Default) Times New Roman, 12 pt

Formatted: Font: (Default) Times New Roman, 12 pt, Not Highlight

Formatted: Font: (Default) Times New Roman, 12 pt

Formatted: Font: (Default) Times New Roman, 12 pt, Not Highlight

Formatted: Font: (Default) Times New Roman, 12 pt

Deleted: ¶

Formatted: German

1180 <https://doi.org/10.1146/annurev.marine.010908.163834>, 2009.

1181

1182 [Du, M. et al. High resolution measurements of methane and carbon dioxide in surface waters](#)

1183 [over a natural seep reveal dynamics of dissolved phase air–sea flux. Environ. Sci. Technol. 48,](#)

1184 [10165–10173 \(2014\).](#)

1185

1186 Fiedler, B., Fietzek, P., Vieira, N., Silva, P., Bittig, H. C., and Körtzinger, A.: In situ CO₂ and O₂

1187 measurements on a profiling float, J. Atmospheric Ocean. Technol., 30, 112–126,

1188 <https://doi.org/10.1175/JTECH-D-12-00043.1>, 2013.

1189

1190 Fietzek, P., Fiedler, B., Steinhoff, T., and Körtzinger, A.: In situ quality assessment of a novel

1191 underwater pCO₂ sensor based on membrane equilibration and NDIR spectrometry, J.

1192 Atmospheric Ocean. Technol., 31, 181–196, <https://doi.org/10.1175/JTECH-D-13-00083.1>,

1193 2014.

1194

1195 Garcia-Tigreros, F., Leonte, M., Ruppel, C. D., Ruiz-Angulo, A., Joung, D. J., Young, B., and

1196 Kessler, J. D.: Estimating the Impact of Seep Methane Oxidation on Ocean pH and Dissolved

1197 Inorganic Radiocarbon Along the U.S. Mid-Atlantic Bight, J. Geophys. Res. Biogeosciences,

1198 126, e2019JG005621, <https://doi.org/10.1029/2019JG005621>, 2021.

1199

1200 Goodman, S., Davies, P., Maddox, M., and Durkee, J.: Arctic Methane – Situational Awareness,

1201 Assessment and Policy Directions, Results of the June 23rd, 2022 Arctic Methane Workshop,

1202 Summary Report, 2022.

Formatted: German

Formatted: Widow/Orphan control, Border: Top: (No border), Bottom: (No border), Left: (No border), Right: (No border), Between : (No border)

1203

1204 Gruber, N., Clement, D., Carter, B. R., Feely, R. A., van Heuven, S., Hoppema, M., Ishii, M.,
1205 Key, R. M., Kozyr, A., Lauvset, S. K., Lo Monaco, C., Mathis, J. T., Murata, A., Olsen, A.,
1206 Perez, F. F., Sabine, C. L., Tanhua, T., and Wanninkhof, R.: The oceanic sink for anthropogenic
1207 CO₂ from 1994 to 2007, *Science*, 363, 1193–1199, <https://doi.org/10.1126/science.aau5153>,
1208 2019.

1209

1210 Gruber, N., Boyd, P. W., Frölicher, T. L., and Vogt, M.: Biogeochemical extremes and
1211 compound events in the ocean, *Nature*, 600, 395–407, [https://doi.org/10.1038/s41586-021-](https://doi.org/10.1038/s41586-021-03981-7)
1212 [03981-7](https://doi.org/10.1038/s41586-021-03981-7), 2021.

1213

1214 Hauri, C., McDonnell, A., Winsor, P., Irving, B., and Statscewich, H.: Development of an
1215 Autonomous Carbon Glider to Monitor Sea-Air CO₂ Fluxes in the Chukchi Sea, Bureau of
1216 Ocean Energy Management, 2018.

1217

1218 [Hauri, C., Irving, B., Hayes, D., Abdi, E., Kemme, J., Kinski, N., McDonnell, A.M.P.: CO₂](#)
1219 [Seaglider trajectory file from Gulf of Alaska 2022. SEANOE. <https://doi.org/10.17882/100964>,](#)
1220 [2022.](#)

1221

1222 [Hauri, C., Irving, B., Hayes, D., Abdi, E., Kemme, J., Kinski, N., McDonnell, A.M.P.: CO₂](#)
1223 [Seaglider trajectory file from Gulf of Alaska 2023. SEANOE. <https://doi.org/10.17882/100965>,](#)
1224 [2023.](#)

1225

Deleted: ¶

1227 Hauri, C., Pagès, R., Hedstrom, K., Doney, S. C., Dupont, S., Ferriss, B., and Stuecker, M. F.:
1228 More Than Marine Heatwaves: A New Regime of Heat, Acidity, and Low Oxygen Compound
1229 Extreme Events in the Gulf of Alaska, AGU Adv., 5, e2023AV001039,

1230 <https://doi.org/10.1029/2023AV001039>, 2024.

1231
1232 Hemming, M. P., Kaiser, J., Heywood, K. J., Bakker, D. C. E., Boutin, J., Shitashima, K., Lee,
1233 G., Legge, O., and Onken, R.: Measuring pH variability using an experimental sensor on an
1234 underwater glider, Ocean Sci., 13, 427–442, <https://doi.org/10.5194/os-13-427-2017>, 2017.

1235

1236 [Irving, B., Hauri, C., Hayes, D., Abdi, E., Kinski, N.: Carbon Dioxide SOP, Version 1.0.0.](#)

1237 [\(GitHub Repository, Carbon Dioxide](#)

1238 [SOP, https://britairving.github.io/Carbon_Dioxide_SOP/README.html](https://britairving.github.io/Carbon_Dioxide_SOP/README.html) (last access: 7 July,

1239 [2024](#)).

1240

1241 Islam, F., DeGrandpre, M. D., Beatty, C. M., Timmermans, M.-L., Krishfield, R. A., Toole, J.
1242 M., and Laney, S. R.: Sea surface CO₂ and O₂ dynamics in the partially ice-covered Arctic
1243 Ocean, J. Geophys. Res. Oceans, 122, 1425–1438, <https://doi.org/10.1002/2016JC012162>, 2017.

1244

1245 Jiang, L.-Q., Feely, R. A., Wanninkhof, R., Greeley, D., Barbero, L., Alin, S., Carter, B. R.,
1246 Pierrot, D., Featherstone, C., Hooper, J., Melrose, C., Monacci, N., Sharp, J. D., Shellito, S., Xu,
1247 Y.-Y., Kozyr, A., Byrne, R. H., Cai, W.-J., Cross, J., Johnson, G. C., Hales, B., Langdon, C.,
1248 Mathis, J., Salisbury, J., and Townsend, D. W.: Coastal Ocean Data Analysis Product in North
1249 America (CODAP-NA) – an internally consistent data product for discrete inorganic carbon,

Deleted: ¶

Formatted: Font: (Default) Times New Roman

Formatted: Font: (Default) Times New Roman

Formatted: Font: (Default) Times New Roman

1251 oxygen, and nutrients on the North American ocean margins, *Earth Syst. Sci. Data*, 13, 2777–
1252 2799, <https://doi.org/10.5194/essd-13-2777-2021>, 2021.

1253

1254 Johnson, G. C. and Lyman, J. M.: Warming trends increasingly dominate global ocean, *Nat.*
1255 *Clim. Change*, 10, 757–761, <https://doi.org/10.1038/s41558-020-0822-0>, 2020.

1256

1257 [Kessler, J. Atlantic bubble bath. *Nature Geosci* 7, 625–626, <https://doi.org/10.1038/ngeo2238>,](https://doi.org/10.1038/ngeo2238)

1258 [2014.](https://doi.org/10.1038/ngeo2238)

1259

1260 Kroeker, K. J., Kordas, R. L., and Harley, C. D. G.: Embracing interactions in ocean
1261 acidification research: Confronting multiple stressor scenarios and context dependence, *Biol.*
1262 *Letts.*, 13, <https://doi.org/10.1098/rsbl.2016.0802>, 2017.

1263

1264 Laufkötter, C., Zscheischler, J., and Frölicher, T. L.: High-impact marine heatwaves attributable
1265 to human-induced global warming, *Science*, 369, 1621–1625,
1266 <https://doi.org/10.1126/science.aba0690>, 2020.

1267

1268 Lauvset, S. K., Lange, N., Tanhua, T., Bittig, H. C., Olsen, A., Kozyr, A., Alin, S., Álvarez, M.,
1269 Azetsu-Scott, K., Barbero, L., Becker, S., Brown, P. J., Carter, B. R., da Cunha, L. C., Feely, R.
1270 A., Hoppema, M., Humphreys, M. P., Ishii, M., Jeansson, E., Jiang, L.-Q., Jones, S. D., Lo
1271 Monaco, C., Murata, A., Müller, J. D., Pérez, F. F., Pfeil, B., Schirnack, C., Steinfeldt, R.,
1272 Suzuki, T., Tilbrook, B., Ulfso, A., Velo, A., Woosley, R. J., and Key, R. M.:

1273 *GLODAPv2.2022: the latest version of the global interior ocean biogeochemical data product,*

Formatted: Font: Times New Roman

Formatted: Hyperlink, Font: Times New Roman, Font color: Auto, Pattern: Clear

Formatted: Widow/Orphan control, Border: Top: (No border), Bottom: (No border), Left: (No border), Right: (No border), Between : (No border)

Field Code Changed

1274 Earth Syst. Sci. Data, 14, 5543–5572, <https://doi.org/10.5194/essd-14-5543-2022>, 2022.

1275

1276 Lee, K., Kim, T.-W., Byrne, R. H., Millero, F. J., Feely, R. A., and Liu, Y.-M.: The universal

1277 ratio of boron to chlorinity for the North Pacific and North Atlantic oceans, *Geochim.*

1278 *Cosmochim. Acta*, 74, 1801–1811, <https://doi.org/10.1016/j.gca.2009.12.027>, 2010.

1279

1280 [Leonte, M., Kessler, J. D., Kellermann, M. Y., Arrington, E. C., Valentine, D. L., Sylva, S. P.,](#)

1281 [Rapid rates of aerobic methane oxidation at the feather edge of gas hydrate stability in the](#)

1282 [waters of Hudson Canyon, US Atlantic Margin. *Geochim. Cosmochim. Acta* 204, 375–387,](#)

1283 <https://doi.org/10.1016/j.gca.2017.01.009>, 2017.

1284

1285 Lueker, T. J., Dickson, A. G., and Keeling, C. D.: Ocean $p\text{CO}_2$ calculated from dissolved

1286 inorganic carbon, alkalinity, and equations for K_1 and K_2 : validation based on laboratory

1287 measurements of CO_2 in gas and seawater at equilibrium, *Mar. Chem.*, 70, 105–119,

1288 [https://doi.org/10.1016/S0304-4203\(00\)00022-0](https://doi.org/10.1016/S0304-4203(00)00022-0), 2000.

1289

1290 Manley, J. and Willcox, S.: The Wave Glider: A persistent platform for ocean science, in:

1291 OCEANS'10 IEEE SYDNEY, OCEANS'10 IEEE SYDNEY, 1–5,

1292 <https://doi.org/10.1109/OCEANSSYD.2010.5603614>, 2010.

1293

1294 [McGinnis, D. F., Greinert, J., Artemov, Y., Beaubien, S. E. & Wüest, A. Fate of rising methane](#)

1295 [bubbles in stratified waters: How much methane reaches the atmosphere? *J. Geophys. Res.* 111,](#)

1296 <https://doi.org/10.1029/2005jc003183>, 2006.

Formatted: English (US)

Formatted: Font: Times New Roman, English (US)

Formatted: English (US)

Formatted: Font: Times New Roman, English (US)

Formatted: English (US)

Formatted: Font: Times New Roman

Formatted: Font: Times New Roman

Formatted: English (US)

Formatted: Line spacing: Double

Formatted: Widow/Orphan control, Border: Top: (No border), Bottom: (No border), Left: (No border), Right: (No border), Between : (No border)

Formatted: Font: Times New Roman, 12 pt

Formatted: Widow/Orphan control, Border: Top: (No border), Bottom: (No border), Left: (No border), Right: (No border), Between : (No border)

1297

1298 Metzl, N., Fin, J., Lo Monaco, C., Mignon, C., Alliouane, S., Antoine, D., Bourdin, G., Boutin,
1299 J., Bozec, Y., Conan, P., Coppola, L., Diaz, F., Douville, E., Durrieu de Madron, X., Gattuso, J.-
1300 P., Gazeau, F., Golbol, M., Lansard, B., Lefèvre, D., Lefèvre, N., Lombard, F., Louanchi, F.,
1301 Merlivat, L., Olivier, L., Petrenko, A., Petton, S., Pujo-Pay, M., Rabouille, C., Reverdin, G.,
1302 Ridame, C., Tribollet, A., Vellucci, V., Wagener, T., and Wimart-Rousseau, C.: A synthesis of
1303 ocean total alkalinity and dissolved inorganic carbon measurements from 1993 to 2022: the
1304 SNAPO-CO2-v1 dataset, *Earth Syst. Sci. Data*, 16, 89–120, [https://doi.org/10.5194/essd-16-89-](https://doi.org/10.5194/essd-16-89-2024)
1305 2024, 2024.

1306

1307 Meurer, W. P., Blum, J., and Shipman, G.: Volumetric Mapping of Methane Concentrations at
1308 the Bush Hill Hydrocarbon Seep, Gulf of Mexico, *Front. Earth Sci.*, 9,
1309 <https://doi.org/10.3389/feart.2021.604930>, 2021.

1310

1311 Monacci, N.M.; Bott, R.; Cross, J.N.; Dougherty, S.; Maenner, S.; Musielewicz, S.; Osborne, J.;
1312 Sutton, A. (2023). High-resolution ocean and atmosphere $p\text{CO}_2$ time-series measurements from
1313 mooring GAKOA_149W_60N. High-resolution ocean and atmosphere $p\text{CO}_2$ time-series
1314 measurements from mooring GAKOA_149W_60N in the Gulf of Alaska (NCEI Accession
1315 0116714). NOAA National Centers for Environmental Information. Dataset.
1316 https://doi.org/10.3334/cdiac/otg.tsm.gakoa_149w_60n

1317

1318 Manley, J. and Willcox, S.: The Wave Glider: A persistent platform for ocean science, in:
 1319 OCEANS'10 IEEE SYDNEY, OCEANS'10 IEEE SYDNEY, 1–5,
 1320 <https://doi.org/10.1109/OCEANSSYD.2010.5603614>, 2010.
 1321
 1322 Miloshevich, L. M., Paukkunen, A., Vömel, H., and Oltmans, S. J.: Development and Validation
 1323 of a Time-Lag Correction for Vaisala Radiosonde Humidity Measurements, *J. Atmospheric*
 1324 *Ocean. Technol.*, 21, 1305–1327, [https://doi.org/10.1175/1520-](https://doi.org/10.1175/1520-0426(2004)021<1305:DAVOAT>2.0.CO;2)
 1325 [0426\(2004\)021<1305:DAVOAT>2.0.CO;2](https://doi.org/10.1175/1520-0426(2004)021<1305:DAVOAT>2.0.CO;2), 2004.
 1326
 1327 [Myhre, G., Shindell, D., Bréon, F.-M., Collins, W., Fuglestedt, J., Huang, J., Koch, D.,](#)
 1328 [Lamarque, J.-F., Lee, D., Mendoza, B., Nakajima, T., Robock, A., Stephens, G., Takemura, T.,](#)
 1329 [and Zhang, H.: Anthropogenic and Natural Radiative Forcing, in: Climate Change 2013: The](#)
 1330 [Physical Science Basis, Contribution of Working Group I to the Fifth Assessment Report of the](#)
 1331 [Intergovernmental Panel on Climate Change, edited by: Stocker, T. F., Qin, D., Plattner, G.-K.,](#)
 1332 [Tignor, M., Allen, S. K., Boschung, J., Nauels, A., Xia, Y., Bex, V., and Midgley, P. M.,](#)
 1333 [Cambridge University Press, Cambridge, UK, New York, NY, USA, 2013.](#)
 1334
 1335 National Academies of Sciences, Engineering, and Medicine: A Research Strategy
 1336 for Ocean-based Carbon Dioxide Removal and Sequestration. Washington, DC: The National
 1337 Academies Press. <https://doi.org/10.17226/26278>, 2022.
 1338
 1339 Newton, J. A., Feely, R. A., Jewett, E. B., Williamson, P., and Mathis, J.: Global ocean
 1340 acidification observing network: requirements and governance plan, GOA-ON, Washington, 61

- Formatted: Font: (Default) Times New Roman, 12 pt
- Formatted: Font: (Default) Times New Roman
- Formatted: Font: (Default) Times New Roman, 12 pt
- Formatted: Line spacing: Double
- Formatted: Font: (Default) Times New Roman
- Formatted: Font: (Default) Times New Roman, 12 pt
- Formatted: Font: (Default) Times New Roman
- Formatted: Font: (Default) Times New Roman, 12 pt
- Formatted: Font: (Default) Times New Roman
- Formatted: Font: (Default) Times New Roman, 12 pt
- Formatted: Font: (Default) Times New Roman
- Formatted: Font: (Default) Times New Roman, 12 pt
- Formatted: Font: (Default) Times New Roman
- Formatted: Font: (Default) Times New Roman, 12 pt
- Formatted: Font: (Default) Times New Roman
- Formatted: Font: (Default) Times New Roman, 12 pt
- Formatted: Font: (Default) Times New Roman
- Formatted: Font: (Default) Times New Roman, 12 pt
- Deleted: ¶

1342 pp., 2015.

1343

1344 Nickford, S., Palter, J. B., Donohue, K., Fassbender, A. J., Gray, A. R., Long, J., Sutton, A. J.,
1345 Bates, N. R., and Takeshita, Y.: Autonomous Wintertime Observations of Air-Sea Exchange in
1346 the Gulf Stream Reveal a Perfect Storm for Ocean CO₂ Uptake, *Geophys. Res. Lett.*, 49,
1347 e2021GL096805, <https://doi.org/10.1029/2021GL096805>, 2022.

1348

1349 von Oppeln-Bronikowski, N., de Young, B., Atamanchuk, D., and Wallace, D.: Glider-based
1350 observations of CO₂ in the Labrador Sea, *Ocean Sci.*, 17, 1–16, [https://doi.org/10.5194/os-17-1-](https://doi.org/10.5194/os-17-1-2021)
1351 2021, 2021.

1352

1353 OceanGliders Oxygen SOP: <https://nora.nerc.ac.uk/id/eprint/533559/>, last access: 24 January
1354 2024.

1355

1356 Orr, J. C., Epitalon, J. M., Dickson, A. G., and Gattuso, J. P.: Routine uncertainty propagation
1357 for the marine carbon dioxide system, *Mar. Chem.*, 207, 84–107,
1358 <https://doi.org/10.1016/j.marchem.2018.10.006>, 2018.

1359

1360 Perez, F. F. and Fraga, F.: Association constant of fluoride and hydrogen ions in seawater, *Mar.*
1361 *Chem.*, 21, 161–168, [https://doi.org/10.1016/0304-4203\(87\)90036-3](https://doi.org/10.1016/0304-4203(87)90036-3), 1987.

1362

1363 Pinnau, I., and Toy, L. G.: Gas and vapor transport properties of amorphous perfluorinated
1364 copolymer membranes based on 2,2-bis(trifluoromethyl)-4,5-difluoro-1,3-

1365 dioxole/tetrafluoroethylene, *Journal of Membrane Science*, 109 (1), 125-133,
1366 [https://doi.org/10.1016/0376-7388\(95\)00193-X](https://doi.org/10.1016/0376-7388(95)00193-X), 1996.
1367
1368 Possenti, L., Humphreys, M. P., Bakker, D. C. E., Cobas-García, M., Fernand, L., Lee, G. A.,
1369 Pallottino, F., Loucaides, S., Mowlem, M. C., and Kaiser, J.: Air-Sea Gas Fluxes and
1370 Remineralization From a Novel Combination of pH and O₂ Sensors on a Glider, *Front. Mar. Sci.*,
1371 8, 1–19, <https://doi.org/10.3389/fmars.2021.696772>, 2021.
1372
1373 [Reeburgh, W. Oceanic methane biogeochemistry. *Am. Chem. Soc.* 107, 486–513, 2007.](#)
1374
1375 [Sarmiento, J. L. and Gruber, N.: *Ocean Biogeochemical Dynamics*, Princeton University Press,](#)
1376 [Princeton, NJ, 526 pp., ISBN 9780691017075, 2006.](#)
1377
1378 Qi, D., Ouyang, Z., Chen, L., Wu, Y., Lei, R., Chen, B., Feely, R. A., Anderson, L. G., Zhong,
1379 W., Lin, H., Polukhin, A., Zhang, Y., Zhang, Y., Bi, H., Lin, X., Luo, Y., Zhuang, Y., He, J.,
1380 Chen, J., and Cai, W. J.: Climate change drives rapid decadal acidification in the Arctic Ocean
1381 from 1994 to 2020, *Science*, 377, 1544–1550, <https://doi.org/10.1126/science.abo0383>, 2022.
1382
1383 Rees, A. P., Bange, H. W., Arévalo-Martínez, D. L., Artioli, Y., Ashby, D. M., Brown, I.,
1384 Campen, H. I., Clark, D. R., Kitidis, V., Lessin, G., Tarran, G. A., and Turley, C.: Nitrous oxide
1385 and methane in a changing Arctic Ocean, *Ambio*, 51, 398–410, [https://doi.org/10.1007/s13280-](https://doi.org/10.1007/s13280-021-01633-8)
1386 [021-01633-8](https://doi.org/10.1007/s13280-021-01633-8), 2022.
1387

Formatted: Font: (Default) Times New Roman, 12 pt

Formatted: Font: Times New Roman, 12 pt

Formatted: Widow/Orphan control, Border: Top: (No border), Bottom: (No border), Left: (No border), Right: (No border), Between : (No border)

Formatted: Font: Times New Roman, 12 pt

1388 Saba, G. K., Wright-Fairbanks, E., Chen, B., Cai, W. J., Barnard, A. H., Jones, C. P., Branham,
1389 C. W., Wang, K., and Miles, T.: The Development and Validation of a Profiling Glider Deep
1390 ISFET-Based pH Sensor for High Resolution Observations of Coastal and Ocean Acidification,
1391 *Front. Mar. Sci.*, 6, 1–17, <https://doi.org/10.3389/fmars.2019.00664>, 2019.

1392

1393 Sabine, C. L. and Tanhua, T.: Estimation of anthropogenic CO₂ inventories in the ocean., *Annu.*
1394 *Rev. Mar. Sci.*, 2, 175–98, <https://doi.org/10.1146/annurev-marine-120308-080947>, 2010.

1395

1396 Sabine, C. L., Feely, R. A., Gruber, N., Key, R. M., Lee, K., Bullister, J. L., Wanninkhof, R.,
1397 Wong, C. S., Wallace, D. W. R., Tilbrook, B., Millero, F. J., Peng, T.-H., Kozyr, A., Ono, T.,
1398 and Rios, A. F.: The oceanic sink for anthropogenic CO₂, *Science*, 305, 367–71,
1399 <https://doi.org/10.1126/science.1097403>, 2004.

1400

1401 Sejr, M. K., Krause-Jensen, D., Rysgaard, S., Sørensen, L. L., Christensen, P. B., and Glud, R.
1402 N.: Air-sea flux of CO₂ in arctic coastal waters influenced by glacial melt water and sea ice,
1403 *Tellus B*, 63, 815–822, <https://doi.org/10.1111/j.1600-0889.2011.00540.x>, 2011.

1404

1405 Sharp, J. D., Pierrot, D., Humphreys, M. P., Epitalon, J.-M., Orr, J. C., Lewis, E. R., and
1406 Wallace, D. W. R.: CO2SYSv3 for MATLAB, , <https://doi.org/10.5281/zenodo.7552554>, 2023.

1407

1408 Shakhova, N., Semiletov, I., Salyuk, A., Yusupov, V., Kosmach, D., and Gustafsson, Ö.:
1409 Extensive Methane Venting to the Atmosphere from Sediments of the East Siberian Arctic Shelf,
1410 *Science*, 327, 1246–1250, <https://doi.org/10.1126/science.1182221>, 2010.

1411

1412 [Skarke, A., Ruppel, C., Kodis, M., Brothers, D. and Lobecker, E. Widespread methane leakage](#)
1413 [from the sea floor on the northern US Atlantic margin. Nat. Geosci. 7, 657 \(2014\).](#)

1414

1415 Sparrow, K. J., Kessler, J. D., Southon, J. R., Garcia-Tigreros, F., Schreiner, K. M., Ruppel, C.

1416 D., Miller, J. B., Lehman, S. J., and Xu, X.: Limited contribution of ancient methane to surface

1417 waters of the U.S. Beaufort Sea shelf, *Sci. Adv.*, 4, eaao4842,

1418 <https://doi.org/10.1126/sciadv.aao4842>, 2018.

1419

1420 Sulpis, O., Lauvset, S. K., and Hagens, M.: Current estimates of K and K appear inconsistent

1421 with measured CO₂ system parameters in cold oceanic regions, *Ocean Sci.*, 16, 847–

1422 862, <https://doi.org/10.5194/os-16-847-2020>, 2020.

1423

1424 Takeshita, Y., Jones, B. D., Johnson, K. S., Chavez, F. P., Rudnick, D. L., Blum, M., Conner, K.,

1425 Jensen, S., Long, J. S., Maughan, T., Mertz, K. L., Sherman, J. T., and Warren, J. K.: Accurate

1426 pH and O₂ Measurements from Spray Underwater Gliders, *J. Atmospheric Ocean. Technol.*, 38,

1427 181–195, <https://doi.org/10.1175/JTECH-D-20-0095.1>, 2021.

1428

1429 Thompson, T., Saba, G. K., Wright-Fairbanks, E., Barnard, A. H., and Branham, C. W.: Best

1430 Practices for Sea-Bird Scientific deep ISFET-based pH sensor integrated into a Slocum Webb

1431 Glider, in: *OCEANS 2021: San Diego – Porto*, *OCEANS 2021: San Diego – Porto*, 1–8,

1432 <https://doi.org/10.23919/OCEANS44145.2021.9706067>, 2021.

1433

Formatted: Widow/Orphan control, Border: Top: (No border), Bottom: (No border), Left: (No border), Right: (No border), Between : (No border)

1434 Vergara-Jara, M. J., DeGrandpre, M. D., Torres, R., Beatty, C. M., Cuevas, L. A., Alarcón, E.,
1435 and Iriarte, J. L.: Seasonal changes in carbonate saturation state and air-sea CO₂ fluxes during an
1436 annual cycle in a stratified-temperate fjord (Reloncaví Fjord, Chilean Patagonia), *J. Geophys.*
1437 *Res. Biogeosciences*, 124, 2851–2865, <https://doi.org/10.1029/2019jg005028>, 2019.

1438

1439 Widdicombe, S., Isensee, K., Artioli, Y., Gaitán-Espitia, J. D., Hauri, C., Newton, J. A.,
1440 et al.: Unifying biological field observations to detect and compare ocean acidification impacts
1441 across marine species and ecosystems: What to monitor and why. *Ocean Science*, **19**(1), 101–
1442 119. <https://doi.org/10.5194/os-19-101-2023>, 2023.

1443

1444 Woosley, R. J. and Millero, F. J.: Freshening of the western Arctic negates anthropogenic carbon
1445 uptake potential, *Limnol. Oceanogr.*, <https://doi.org/10.1002/lno.11421>, 2020.

1446

1447 Wright-Fairbanks, E. K., Miles, T. N., Cai, W.-J., Chen, B., and Saba, G. K.: Autonomous
1448 Observation of Seasonal Carbonate Chemistry Dynamics in the Mid-Atlantic Bight, *J. Geophys.*
1449 *Res. Oceans*, 125, e2020JC016505, <https://doi.org/10.1029/2020JC016505>, 2020.

1450

1451

1452

1453

1454

1455 **Tables**

1456 **Table 1. Tank experiment.** Evaluation of SG HydroC CO₂ and SG HydroC CH₄ sensors
 1457 compared to reference discrete $p\text{CO}_2^{\text{disc}}$ and $p\text{CH}_4^{\text{disc}}$. Units of $p\text{CO}_2$ and $p\text{CH}_4$ are μatm except
 1458 when shown as percent difference in parenthesis (Equation 1). Columns with subscripts sn422
 1459 and sn0718 indicate data from sensors HydroC CO2T-0422-001 and HydroC CO2T-0718-001,
 1460 respectively. Superscript RTC indicates response time corrected values following Dølven et al.
 1461 (2022). $p\text{CO}_2^{\text{disc}}$ and $p\text{CH}_4^{\text{disc}}$ values are the average of triplicate bottles and are shown in Figure
 1462 4.

Commented [MOU5]: Please add new tables and captions

Deleted: calculated with input pairs pH_{lab} and DIC
 Formatted: Superscript
 Formatted: Superscript
 Formatted: Not Superscript/ Subscript

Deleted: Values

1463

Deleted: Discrete Sample # ... [16]

| Triplicate Date Time (UTC) | $p\text{CO}_2^{\text{disc}} \pm \text{uc} (\mu\text{atm})$ | $\frac{p\text{CO}_{2,\text{sn422}}^{\text{RTC}}}{p\text{CO}_2^{\text{disc}}}$ | $\frac{p\text{CO}_{2,\text{sn0718}}^{\text{RTC}}}{p\text{CO}_2^{\text{disc}}}$ | $p\text{CH}_4^{\text{disc}} \pm \text{u} (\mu\text{atm})$ | $p\text{CH}_4^{\text{RTC}} / p\text{CH}_4^{\text{disc}}$ |
|----------------------------|--|---|--|---|--|
| 5/2/2022 3:25 | 298.7 ± 10.2 | -0.9 (0.3 %) | = | = | = |
| 5/2/2022 7:32 | 227.1 ± 7.8 | 4.3 (1.9 %) | 2.4 (1.1 %) | = | = |
| 5/2/2022 11:27 | 223.3 ± 7.7 | 0.7 (0.3 %) | -2.6 (1.2 %) | = | = |
| 5/2/2022 15:30 | 227.8 ± 7.9 | -1.1 (0.5 %) | -3.3 (1.5 %) | = | = |
| 5/2/2022 00:11 | = | = | = | 25.4 ± 2.1 | 4.0 (14.6 %) |
| 5/2/2022 12:06 | = | = | = | 7.3 ± 1.3 | 0.5 (6.3 %) |

Formatted Table
 Formatted: Font: 12 pt
 Formatted: Font: 12 pt
 Formatted: Font: 12 pt
 Formatted: Line spacing: single
 Formatted: Line spacing: single
 Formatted: Line spacing: single
 Formatted: Line spacing: single
 Formatted: Line spacing: single
 Formatted: Line spacing: single
 Formatted: Line spacing: single

1464

1465

1469 **Table 2. Profiling experiment.** Evaluation of SG HydroC CO₂ sensor compared to reference
 1470 discrete $p\text{CO}_2^{\text{disc}}$. Units of $p\text{CO}_2$ are μatm except when shown as percent difference in
 1471 parenthesis (Eq. 1). $p\text{CO}_2$ with subscripts sn422 indicate data from the HydroC installed on the
 1472 rosette (HydroC CO2T-0422-001). The superscript RTC indicates response time corrected values
 1473 following Dølven et al. (2022).

Deleted: ¶

Deleted: calculated with input pair

Deleted: s pH_{lab} and DIC.

Deleted: Asterisks (*) indicate the comparison with rosette mounted SG HydroC CO₂ values taken as nearest in time before sensor zeroing.

| Discrete Date Time (UTC) | Discrete Depth (m) | $p\text{CO}_2^{\text{disc}} \pm \text{uc}$ (μatm) | $p\text{CO}_{2,\text{sn422}}^{\text{RTC}} - p\text{CO}_2^{\text{disc}}$ |
|--------------------------|--------------------|--|---|
| 5/3/2022 21:21 | 2.5 | 214.5 ± 7.5 | 5.4 (2.5%)* |
| 5/3/2022 21:39 | 19.9 | 246.8 ± 8.5 | 1.6 (0.6%)* |
| 5/3/2022 22:33 | 9.6 | 244.4 ± 8.5 | -3.3 (1.4%)* |
| 5/3/2022 22:34 | 9.7 | 234.7 ± 8.1 | 8.2 (3.4%)* |

Deleted: 9.3 (4.2%)*

Formatted Table

Deleted: 3.4 (1.4%)*

Deleted: -2.3 (0.9%)*

Deleted: 7.5 (3.2%)*

1474

1475

1486 **Table 3. Seaglider HydroC evaluation with a nearby cast.** Evaluation of Seaglider integrated
 1487 and rosette mounted SG HydroC CO₂ sensors compared to $p\text{CO}_2^{\text{disc}}$ collected from a nearby cast.
 1488 Units of $p\text{CO}_2$ are μatm except when shown as percent difference in parenthesis (Eq. 1) and
 1489 differences between $p\text{CO}_{2,\text{Seaglider}}^{\text{RTC}}$ were calculated with the average (upcast and downcast
 1490 combined) 1-meter binned data. The superscript RTC indicates response time corrected values
 1491 following Dølven et al. (2022), and subscripts Rosette and Seaglider indicate the SG HydroC
 1492 CO₂ sensor mounted on the rosette (SG HydroC CO2T-0422-001) and integrated into the
 1493 Seaglider (SG HydroC CO2T-0718-001), respectively. Time delay (HH:MM) and spatial
 1494 distance (km) columns represent the distance between $p\text{CO}_{2,\text{Seaglider}}^{\text{RTC}}$ measured at the discrete
 1495 depth and the discrete date time. The asterisk (*) indicates the comparison with $p\text{CO}_{2,\text{Rosette}}^{\text{RTC}}$
 1496 taken as nearest in time before sensor zeroing (Figure S1).

| Discrete Date Time (UTC) | Discrete Depth (m) | $p\text{CO}_2^{\text{disc}} \pm \text{uc}$ (μatm) | $\frac{p\text{CO}_{2,\text{Rosette}}^{\text{RTC}}}{p\text{CO}_2^{\text{disc}}}$ | Delay (HH:MM) | Distance (km) | $\frac{p\text{CO}_{2,\text{Seaglider}}^{\text{RTC}}}{p\text{CO}_2^{\text{disc}}}$ |
|--------------------------|--------------------|--|---|---------------|---------------|---|
| 5/7/2022 18:06 | 71.8 | 349.7 ± 7.8 | -5.7 (1.6 %) | 02:47 | 0.4 | 10.2 (2.9 %) |
| 5/7/2022 18:24 | 57.1 | 313.8 ± 6.7 | 12.1 (3.8 %) | 03:05 | 0.6 | 8.3 (2.6 %) |
| 5/7/2022 18:42 | 19.8 | 285.3 ± 6.1 | 0.8 (0.3 %) | 03:23 | 0.8 | 8.6 (3.0 %) |
| 5/7/2022 19:00 | 1.6 | 233.4 ± 5.0 | -2.3 (1.0 %)* | 03:41 | 0.9 | 12.0 (5.0 %) |

Deleted: ¶

Formatted: Font: 12 pt

Formatted: Font: 12 pt

Formatted: Font: 12 pt

Formatted: Font: 12 pt

Formatted: Font: 12 pt

Formatted: Font: 12 pt

Formatted: Font: 12 pt

Formatted: Font: 12 pt

Deleted: Evaluation of Seaglider integrated SG HydroC CO₂ sensor compared to discrete $p\text{CO}_2^{\text{disc}}$ calculated with input pairs pH_{lab} and DIC collected from a rosette nearby. Units of $p\text{CO}_2$ are μatm except when shown as percent difference in parenthesis (Eq. 1). The superscript RTC indicates response time corrected values following Dølven et al. (2022). Distance columns represent the distance between when $p\text{CO}_2$ was measured on the Seaglider integrated HydroC to the time the discrete sample was collected and is given temporally (HH:MM) and spatially (km). $p\text{CO}_{2,\text{sn422}}^{\text{RTC}}$ is the rosette mounted SG HydroC CO₂ sensor and $p\text{CO}_{2,\text{sn0718}}^{\text{RTC}}$ is the Seaglider mounted SG HydroC CO₂ sensor.

Formatted: Font: 12 pt

Formatted Table

Deleted: sn0718

Formatted: Font: 12 pt

Deleted: 2.5

Deleted: 9.5

Deleted: 7

Deleted: 7

Deleted: 6.6

Deleted: 1

Deleted: 20

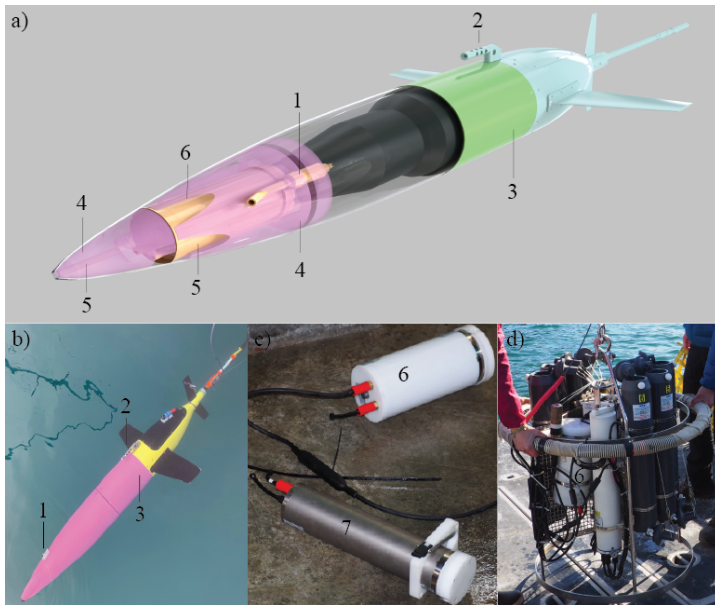
Deleted: 15.1

Deleted: 6.3

1497

1498

1522 **Figures**



1523

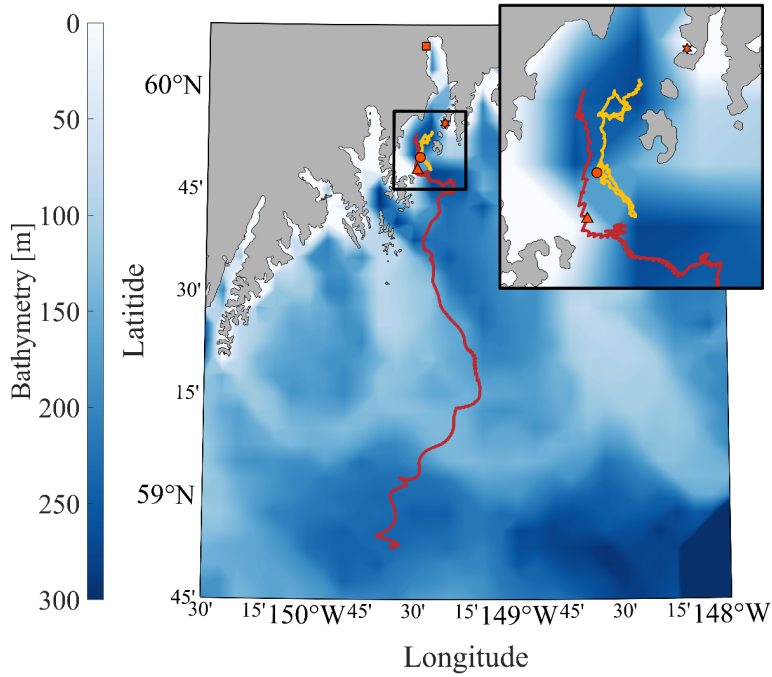
1524 **Figure 1. CO₂ Seaglider.** CO₂ Seaglider a) schematic rendering and b) picture in Resurrection
1525 Bay, Seward, Alaska, during a checkout dive on 6 February, 2023, before beginning the first
1526 winter mission collecting high resolution *p*CO₂ data. Highlighted are 1) SeaBird 5M pump, 2)
1527 conductivity and temperature sail, 3) extension, 4) syntactic foam, 5) water flow channels, and 6)
1528 SG HydroC CO₂ in a titanium housing, enabling *p*CO₂ observations down to 1000 m. c) Picture
1529 of new SG HydroC CO₂ in a POM housing (6, rated to 300 m depth) and original CONTROS
1530 HydroC™ CO₂ (7). d) Picture of rosette set up for profiling experiment.

Formatted: Font: Italic



1531

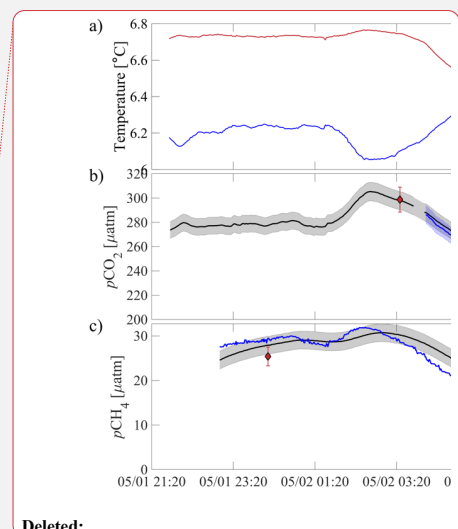
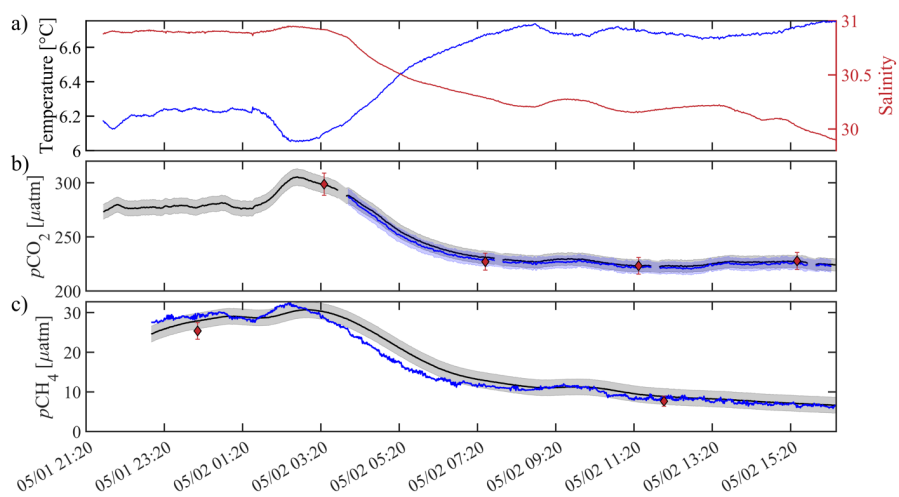
1532 **Figure 2. SG HydroC CO₂ sensor mounting designs.** a) Titanium SG HydroC CO₂ (rated to
1533 1000m) in a custom syntactic foam coat and b) POM SG HydroC CO₂ (rated to 300m) with
1534 brackets.



1535

1536 **Figure 3. Map of CO₂ Seaglider study area.** The bathymetry of the Gulf of Alaska is shown in
 1537 color with zoomed in section of the head of Resurrection Bay (outlined black square and inset
 1538 map). Tracks of the CO₂ Seaglider from the May 2022 and February 2023 missions are shown in
 1539 yellow and red, respectively. Orange markers outlined in black show the location of the Alutiiq
 1540 Pride Marine Institute (square), National Oceanic and Atmospheric Administration’s Gulf of
 1541 Alaska Ocean Acidification mooring (star), May 7th CTD cast (circle), and last location where
 1542 *p*CO₂ was collected during the February 2023 mission (triangle).

1543



1544

1545 **Figure 4. Sensor validation during a tank experiment at the Alutiiq Pride Marine Institute**
 1546 **on May 1 – 2, 2022.** a) temperature (blue line) and salinity (red line) from a recently calibrated
 1547 Sea-Bird Scientific SBE37. b) black (blue) lines show $p\text{CO}_2$ in μatm from HydroC CO2T-0422-
 1548 001 (HydroC CO2T-0718-001) with the shaded gray (blue) areas showing a relative uncertainty
 1549 of 2.5% (weather quality goal; Newton et al., 2015). Black circles with red filling show discrete
 1550 $p\text{CO}_2^{\text{disc}}$ with error bars showing the combined standard uncertainty from *errors.m* (Orr et al.,
 1551 2018). HydroC $p\text{CO}_2$ data are shown at 1 minute resolution with a 2-minute moving median
 1552 filter applied and have not been corrected for response time, but differences were negligible (\leq
 1553 $0.1 \mu\text{atm}$). c) Black line shows $p\text{CH}_4$ in μatm from HydroC CH4T-0422-001 with the shaded
 1554 gray bar showing an uncertainty of $2 \mu\text{atm}$. The blue line is the response time corrected signal
 1555 with a response time of 43 minutes following Dølven et al., (2022). HydroC $p\text{CH}_4$ data are
 1556 shown at 1 minute resolution with a 2-minute moving median filter applied to the raw data and a

Deleted:

Deleted: calculated from input pair pH_{lab} and DIC

Deleted: are

Deleted: Table 1

Deleted: (published instrument accuracy of $\pm 2 \mu\text{atm}$ or $\pm 3\%$, whichever is greater).

1563 10-minute moving median filter applied to the RTC data. Black diamonds with red filling show
1564 discrete $p\text{CH}_4^{\text{disc}}$ and all discrete values of $p\text{CO}_2^{\text{disc}}$ and $p\text{CH}_4^{\text{disc}}$ are the average of triplicate
1565 bottles.

Deleted: circles

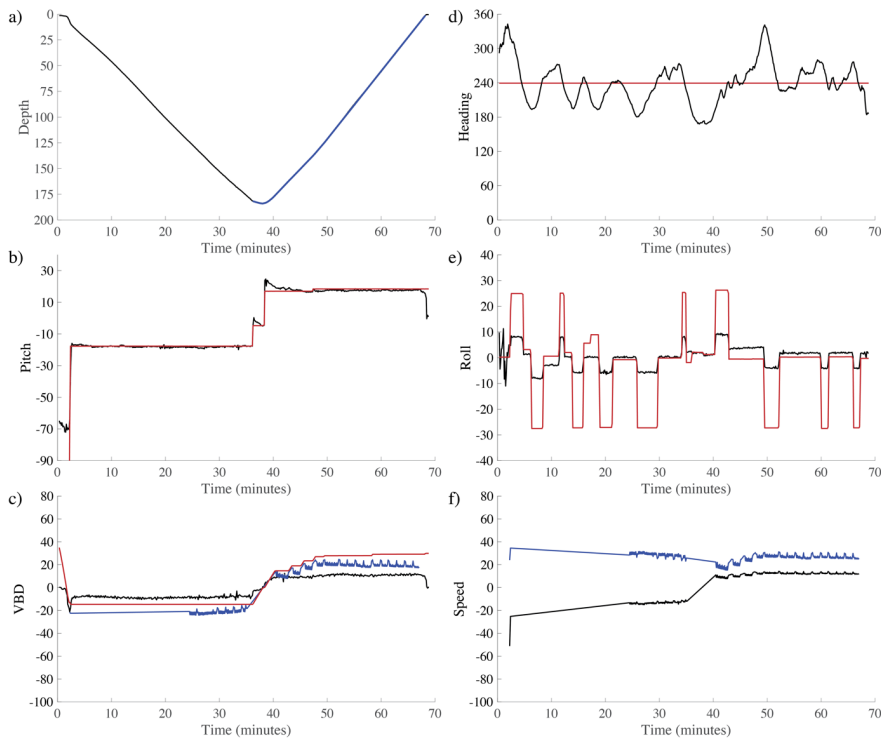
Formatted: Superscript

Formatted: Superscript

Formatted: Superscript

1566

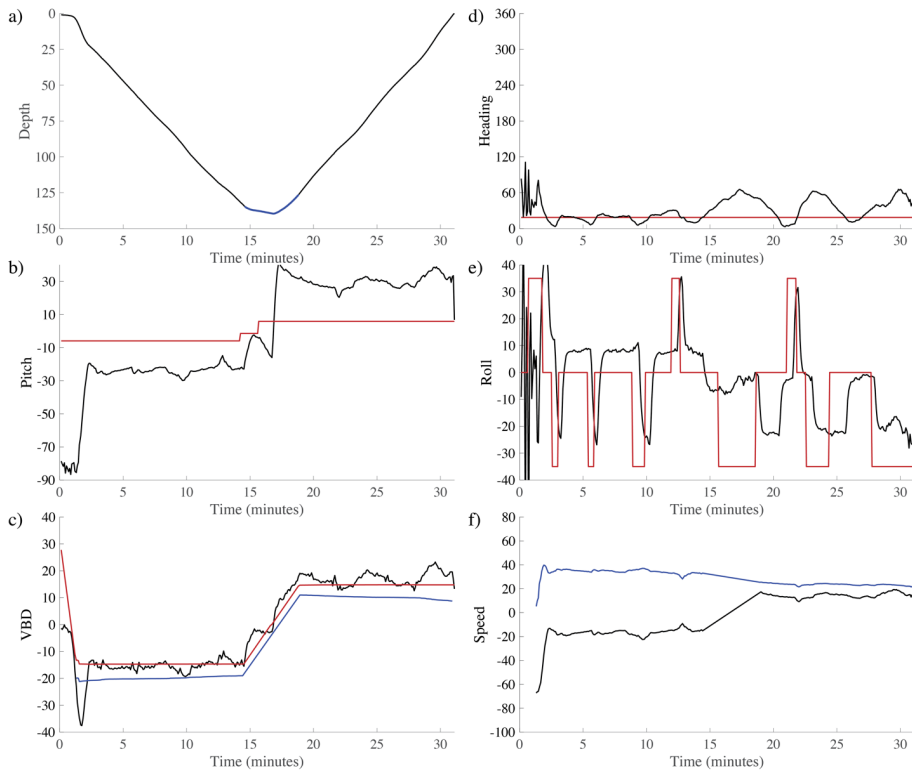
1568



1569

1570 **Figure 5. Dive details for the 300 m rated CO₂ Seaglider (dive# 51).** a) Depth (black line,
1571 meters), b) pitch (black line, degrees) with pitch control (red line, mm of battery shift), c)
1572 Change in displacement of Variable Buoyancy Drive (VBD) (red line, units of 10 cc), vertical
1573 velocity from pressure measurements (black line, cm/s), and buoyancy (blue line, units of 10 g),
1574 d) heading in (desired red line, measured black line, degrees), e) roll (battery roll position red
1575 line, glider measured roll black line, degrees), and f) vertical speed (calculated from buoyancy
1576 and pitch, black line, cm/s) and horizontal speed (calculated from buoyancy and pitch, blue line,
1577 cm/s).

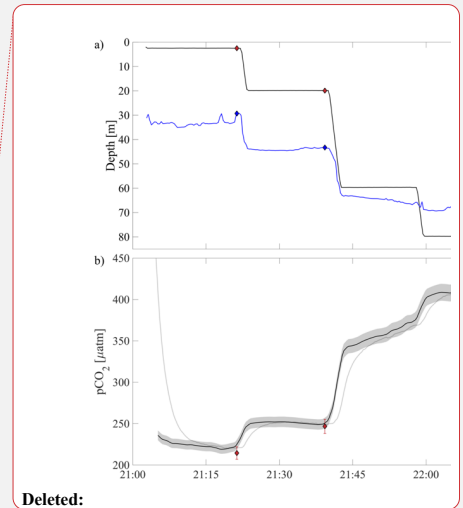
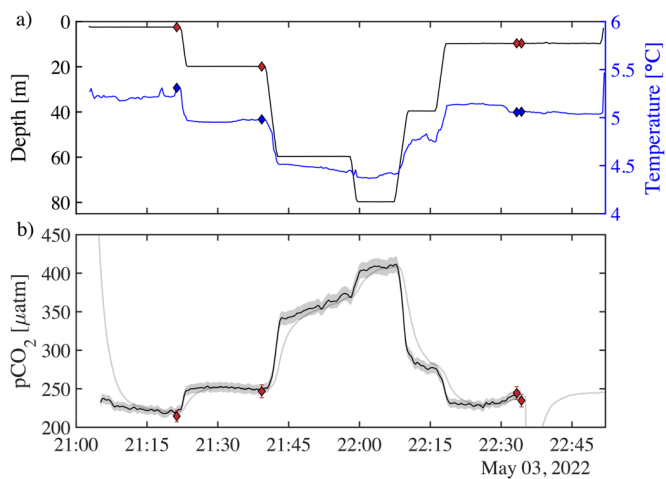
Deleted: plot



1579

1580 **Figure 6. Dive details for the 1000 m rated CO₂ Seaglider (dive# 203).** a) Depth (black line,
 1581 meters), b) pitch (black line, degrees) with pitch control (red line, mm of battery shift), c)
 1582 Change in displacement of Variable Buoyancy Drive (VBD) (red line, units of 10 cc), vertical
 1583 velocity from pressure measurements (black line, cm/s), and buoyancy (blue line, units of 10 g),
 1584 d) Heading (desired heading red line, measured heading black line, degrees) e) roll (battery roll
 1585 position red line, glider measured roll black line, degrees), and f) vertical speed (calculated from
 1586 buoyancy and pitch, black line, cm/s) and horizontal speed in cm/s (calculated from buoyancy
 1587 and pitch, blue line, cm/s).

Deleted: plot



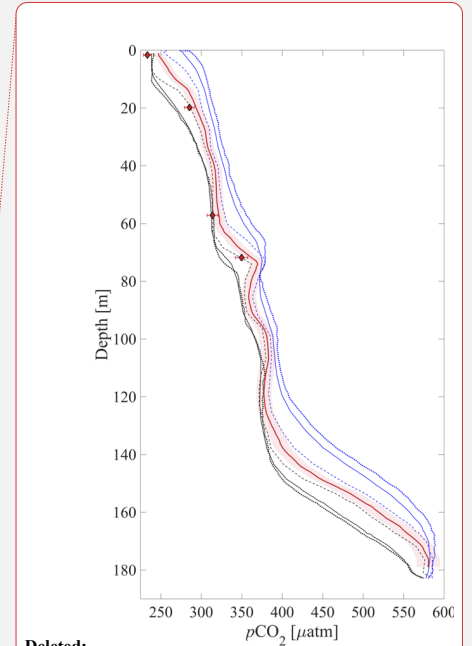
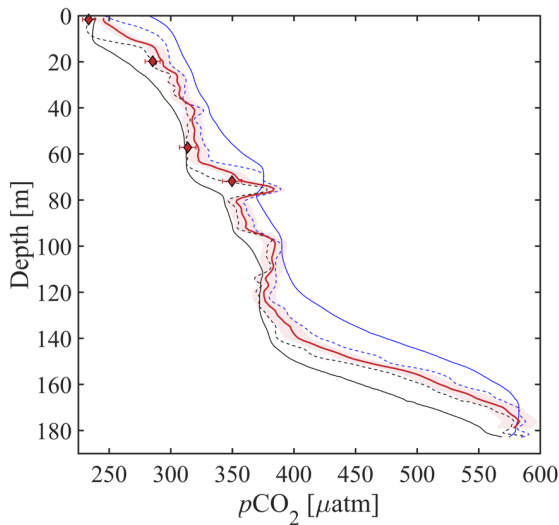
1589

1590 **Figure 7. Profiling experiments from May 3rd with HydroC CO2T-0422-001 sensor**

1591 **mounted on the rosette.** a) Pressure vs time on the left (black) axis with diamonds showing
 1592 rosette CTD values of pressure (red filled diamond), and temperature vs time on the right (blue)
 1593 axis and temperature (blue filled diamond) at the time of the bottle fire. b) $p\text{CO}_2$ measured by
 1594 the rosette mounted SG HydroC CO_2 sensor as raw (gray line) and response time corrected
 1595 signal (thick black line; $p\text{CO}_{2,\text{sn422}}^{\text{RTC}}$ in Table 2) with shaded relative uncertainty of 2.5%
 1596 (weather goal; Newton et al., 2015). $p\text{CO}_2^{\text{disc}}$ shown as red diamonds with vertical red error bars
 1597 showing combined standard uncertainty (Orr et al., 2018). Table 2 shows differences between
 1598 discrete $p\text{CO}_2^{\text{disc}}$ and $p\text{CO}_{2,\text{sn422}}^{\text{RTC}}$. The SG HydroC CO_2 sensor started a zeroing interval at
 1599 22:35 on May 3, 2022, so $p\text{CO}_{2,\text{sn422}}^{\text{RTC}}$ is not shown after that time but signal recovery can be
 1600 seen in the uncorrected signal (gray line).

1601

- Deleted: Discrete
- Deleted:
- Deleted: (pH_{lab}, DIC)
- Formatted: Superscript
- Deleted:
- Deleted: (pH_{lab}, DIC)
- Deleted: the
- Deleted: HydroC $p\text{CO}_2^{\text{RTC}}$ signal
- Formatted: Superscript
- Deleted: so RTC $p\text{CO}_2$



1612

1613 **Figure 8. CO₂ Seaglider data from a sea trial mission in [May 2022](#) in Resurrection Bay,**
 1614 **Seward, Alaska. [Depth profile of pCO₂ in µatm showing the original resolution smoothed pCO₂](#)**
 1615 **[used in the RT correction \(downcast = solid black, upcast = solid blue\), RTC pCO₂ following](#)**
 1616 **[Dølven et al. \(2022\) \(dashed black line = downcast, dashed blue line = upcast\), and 1-meter](#)**
 1617 **[binned RTC profile \(thick red line\) with red shading showing the relative uncertainty of 2.5 %.](#)**
 1618 **[Discrete pCO₂^{disc} shown as red diamonds with horizontal red error bars showing combined](#)**
 1619 **[standard uncertainty \(Orr et al., 2018\). Differences between pCO₂^{disc} and pCO_{2,Seaglider}^{RTC} are](#)**
 1620 **[shown in Table 3.](#)**

1621

1622

Deleted:

Deleted: spring

Formatted: Space Before: Auto, Line spacing: Double

Formatted: Font: 12 pt

Formatted: Font: 12 pt

Formatted: Font: 12 pt

Deleted: (pH_{lab}, DIC)

Formatted: Font: 12 pt

Deleted: discrete

Deleted: RTC

Deleted: is

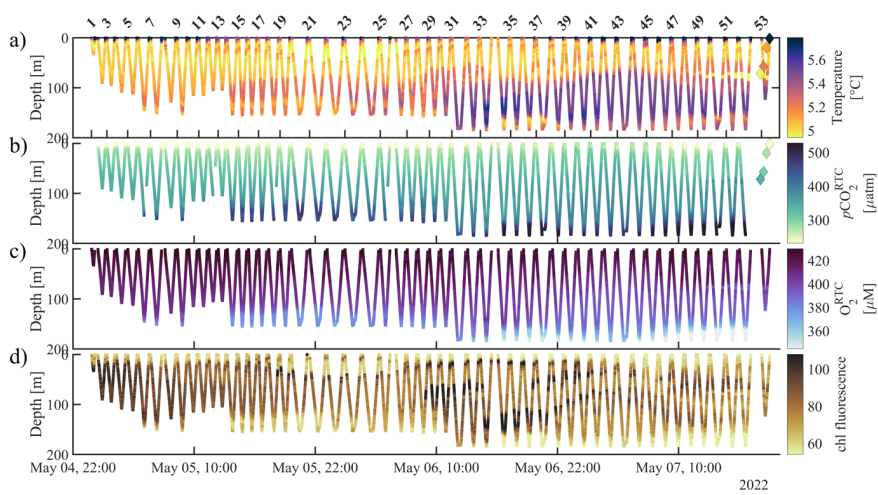
Formatted: Font: 12 pt

Formatted: Font: 12 pt

Formatted: Superscript

Formatted: Font color: Black

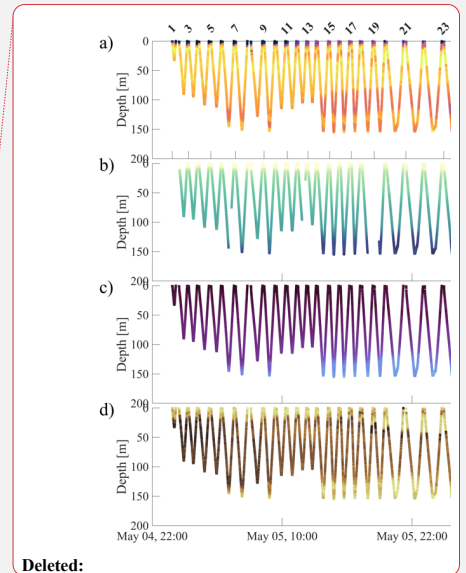
Deleted: Depth profile of pCO₂ in µatm showing downcast (dotted black is the original resolution, solid black is the 1 minute averaged downcast), upcast (dotted blue is the original resolution, solid blue is the 1 minute averaged upcast), RTC pCO₂ following Dølven et al. (2022) (dashed black line = downcast, dashed blue line = upcast) and ... [17]



1645

1646 **Figure 9. CO₂ Seaglider data from a sea trial mission in spring 2022 in Resurrection Bay,**
 1647 **Seward, Alaska.** Depth profiles of a) Temperature [°C], b) RTC $p\text{CO}_2$ [μatm] c) RTC O_2 [μM],
 1648 and d) raw chlorophyll fluorescence. The [diamonds](#) show discrete values that were taken during
 1649 a CTD cast (Table 3).

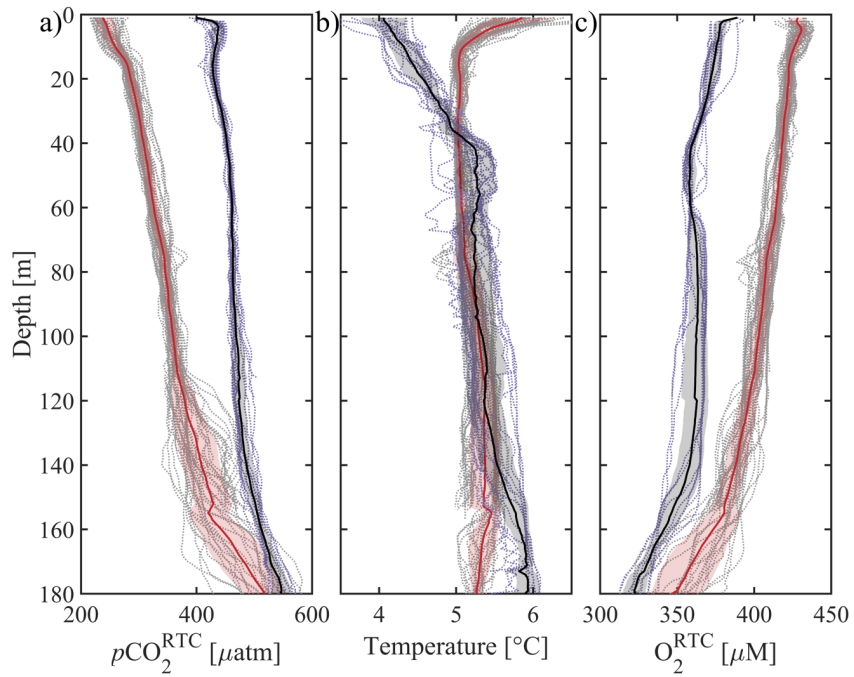
1650



Deleted:

Deleted: triangles

Deleted:



1654

1655

1656 **Figure 10. Averaged CO₂ Seaglider profiles from May 2022 and February 2023 missions in**

1657 **Resurrection Bay, Seward, Alaska.** Depth profiles of all 1-meter binned dives (dotted gray),

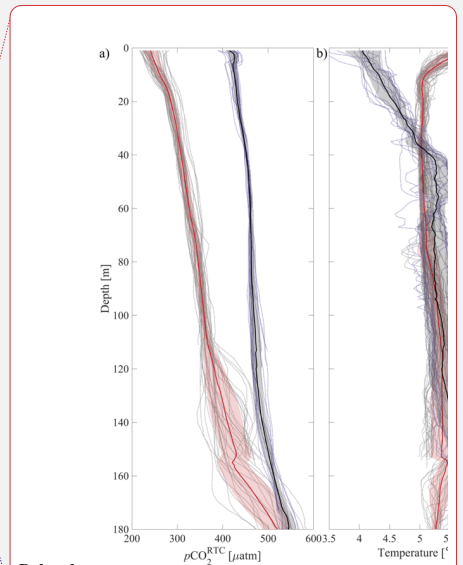
1658 average 1-meter binned dive from May 2022 mission (red thick line, dive#1-51, May 5, 2022

1659 00:01 to May, 7 2022 16:37) and February 2023 mission (black thick line, dive#1-17, February

1660 8, 2023 20:50 to February 9, 2023 19:54) [with shading showing the standard deviation of the](#)

1661 [values in each bin added and subtracted from the average.](#) a) Response time corrected $p\text{CO}_2$

1662 ($p\text{CO}_2^{\text{RTC}}$, μatm), b) temperature [$^{\circ}\text{C}$], and c) response time corrected oxygen (O_2^{RTC} , μM).

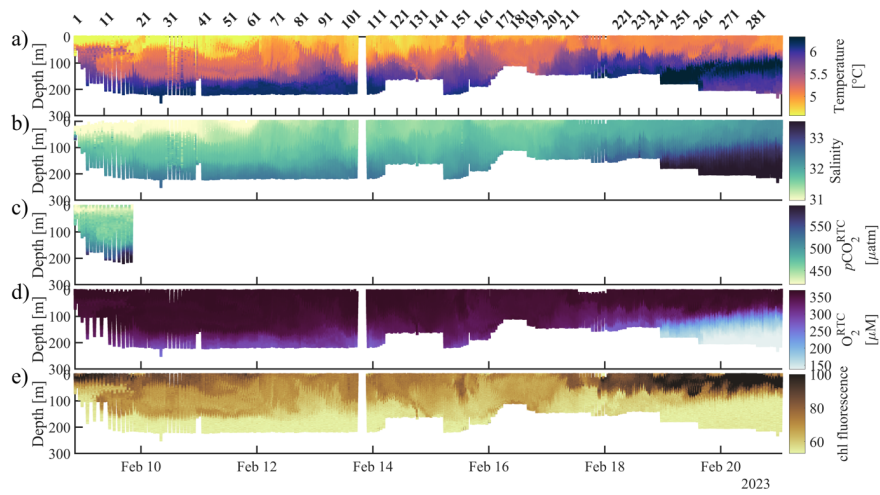


Deleted:

Deleted: 53

Deleted: with shading showing the standard deviation of the average....

1667



1668

1669 **Figure 11. CO₂ Seaglider data collected during the winter mission (February 8 - 21, 2023).**

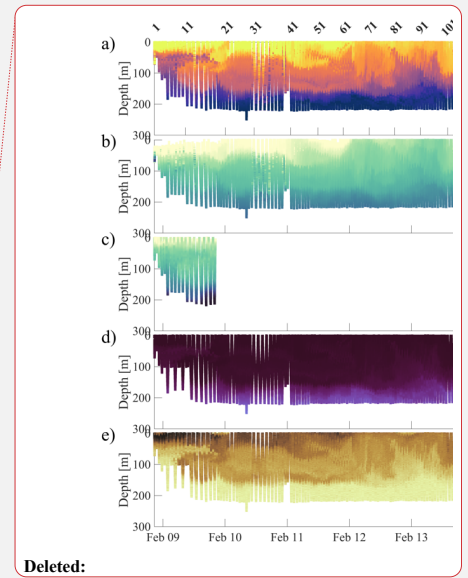
1670 Shown are a) temperature (°C), b) salinity, c) response time corrected $p\text{CO}_2$ ($p\text{CO}_2^{\text{RTC}}$, μatm), d)

1671 response time corrected oxygen (O_2^{RTC} , μM), and e) raw chlorophyll fluorescence (chl

1672 fluorescence) as time/dive number vs. pressure.

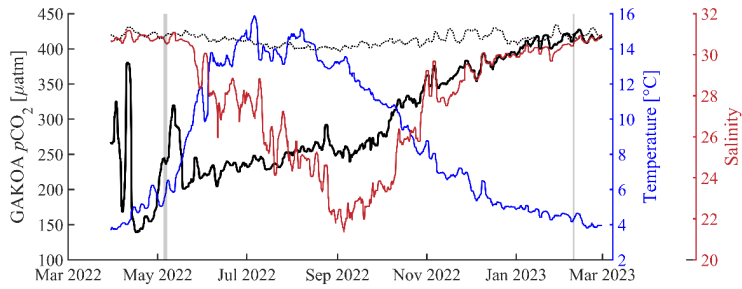
1673

1674



Deleted:

Deleted: 20



1677

1678 **Figure 12. National Oceanic Atmospheric Administration’s Gulf of Alaska ocean**
 1679 **acidification surface time-series from March 2022 - 2023.** Left axis [sea](#) surface (dotted black
 1680 line) and air (black line, 4 meter above sea level) $p\text{CO}_2$ [μatm] and right axes sea surface
 1681 temperature (blue, $^{\circ}\text{C}$) and sea surface salinity (red). All data shown as 3 day running mean.
 1682 Vertical shaded gray areas highlight the CO_2 Seaglider missions in May 2022 and February
 1683 2023. The mooring is located at 59.911°N , -149.35°W (Monacci et al., 2023).

1684

1685

1686

1687

Page 16: [1] Deleted Brita Irving 6/24/24 11:31:00 AM

Page 16: [2] Deleted Microsoft Office User 6/6/24 7:23:00 AM

Page 16: [3] Deleted Microsoft Office User 6/6/24 7:15:00 AM

Page 16: [4] Formatted Microsoft Office User 6/6/24 12:59:00 PM

Font: (Default) Times New Roman, Not Italic, Subscript

Page 17: [5] Formatted Microsoft Office User 6/6/24 12:59:00 PM

Font: (Default) Times New Roman, Not Italic

Page 17: [5] Formatted Microsoft Office User 6/6/24 12:59:00 PM

Font: (Default) Times New Roman, Not Italic

Page 17: [6] Formatted Microsoft Office User 6/6/24 12:59:00 PM

Font: (Default) Times New Roman, Not Italic

Page 17: [6] Formatted Microsoft Office User 6/6/24 12:59:00 PM

Font: (Default) Times New Roman, Not Italic

Page 17: [6] Formatted Microsoft Office User 6/6/24 12:59:00 PM

Font: (Default) Times New Roman, Not Italic

Page 17: [6] Formatted Microsoft Office User 6/6/24 12:59:00 PM

Font: (Default) Times New Roman, Not Italic

Page 17: [6] Formatted Microsoft Office User 6/6/24 12:59:00 PM

Font: (Default) Times New Roman, Not Italic

Page 17: [7] Formatted Microsoft Office User 6/6/24 12:59:00 PM

Font: 12 pt

Page 17: [7] Formatted Microsoft Office User 6/6/24 12:59:00 PM

Font: 12 pt

Page 17: [7] Formatted Microsoft Office User 6/6/24 12:59:00 PM

Font: 12 pt

Page 17: [7] Formatted Microsoft Office User 6/6/24 12:59:00 PM

Font: 12 pt

Page 17: [8] Formatted Microsoft Office User 6/14/24 1:03:00 PM

Font: Times New Roman, 12 pt

Page 17: [8] Formatted Microsoft Office User 6/14/24 1:03:00 PM

Font: Times New Roman, 12 pt

Page 17: [9] Deleted Microsoft Office User 6/6/24 7:24:00 AM

Page 17: [10] Formatted Microsoft Office User 6/6/24 1:08:00 PM

Font: (Default) Times New Roman, 12 pt, Not Bold

Page 17: [11] Formatted Microsoft Office User 6/6/24 1:08:00 PM

Font: (Default) Times New Roman, 12 pt, Not Bold

Page 17: [12] Deleted Claudine Hauri 6/26/24 6:23:00 AM

Page 17: [12] Deleted Claudine Hauri 6/26/24 6:23:00 AM

Page 17: [13] Formatted Microsoft Office User 6/6/24 1:08:00 PM

Font: (Default) Times New Roman, 12 pt, Not Bold

Page 17: [13] Formatted Microsoft Office User 6/6/24 1:08:00 PM

Font: (Default) Times New Roman, 12 pt, Not Bold

Page 17: [13] Formatted Microsoft Office User 6/6/24 1:08:00 PM

Font: (Default) Times New Roman, 12 pt, Not Bold

Page 17: [13] Formatted Microsoft Office User 6/6/24 1:08:00 PM

Font: (Default) Times New Roman, 12 pt, Not Bold

Page 17: [13] Formatted Microsoft Office User 6/6/24 1:08:00 PM

Font: (Default) Times New Roman, 12 pt, Not Bold

Page 17: [14] Formatted Brita Irving 6/24/24 11:37:00 AM

No underline

Page 17: [14] Formatted Brita Irving 6/24/24 11:37:00 AM

No underline

Page 17: [14] Formatted Brita Irving 6/24/24 11:37:00 AM

No underline

Page 17: [14] Formatted Brita Irving 6/24/24 11:37:00 AM

No underline

Page 17: [15] Formatted Microsoft Office User 6/6/24 1:08:00 PM

Font: (Default) Times New Roman, 12 pt, Not Bold

Page 44: [16] Deleted Brita Irving 6/18/24 1:29:00 PM

Page 55: [17] Deleted Microsoft Office User 6/14/24 1:25:00 PM